Università degli Studi di Catania
Scuola Superiore di Catania

International PhD

in

Nanoscience

XXIV cycle

Ultrasensitive methods for the detection of biomolecular systems at the micro/nano scale

Laura Maria Zanoli

Coordinator of PhD

Prof.ssa Maria Grazia Grimaldi

Tutor

Prof. Giuseppe Spoto

a.a. 2008/2011

CONTENTS

ABSTRACT

A great effort has been devoted, during the past decade, to the development of new devices for specific DNA sequences detection, due to the relevance of nucleic acid analysis in many areas, including clinical diagnostics, environmental monitoring and food-quality control. However, diagnostic tools used for the detection of nucleic acids need to fulfil specific requirements in term of sensitivity, selectivity and high-throughput in order to expand their applicability and to minimize the cost of the assay. In fact, very small amount of DNA is typically available for the analysis and a detection scheme capable of directly transducing the hybridization events with a proper sensitivity is required. In addition, the sequence to be targeted is often present in a complex environment such as the whole genomic DNA and the use of very specific and highly efficient probes is required in order to build highly selective detection scheme.

The purpose of my research activity was the identification of new methodologies useful for DNA detection with the principal aim to perform the analysis with a very small amount of samples. In this perspective, interesting results were obtained by using microfluidic systems, characterized by the presence of one or more microchannels where fluid reagents are easily and carefully manipulated. In particular, the combined use of a droplet-based microfluidics, PNA-MBs and fluorescence microscopy enabled the selective and sensitive detection of DNA in an innovative and efficient platform. The experiments were carried out by using both oligonucleotides and PCR amplification products and were aimed at detecting DNA sequences of different olive cultivar.

The ultrasensitive detection of DNA was also investigated by coupling microfluidic devices with the SPRi apparatus. A similar approach allowed a real time

label-free detection of specific genomic DNA sequences carrying the β°39 thalassemia mutation. The capacity in term of selectivity and sensitivity was investigated by employing surface-immobilized PNA probes in combination with gold nanoparticle-enhanced SPRi detection. The DNA concentrations measured by this method are in a range suitable for detecting DNA samples without amplification.

1. INTRODUCTION

Diagnostic tools used for the detection of biomolecules need to fulfil specific requirements in term of sensitivity, selectivity and high-throughput in order to expand their applicability and to minimize the cost of the assay.[1]

The typical approach for the detection of DNA requires both the amplification by polymerase chain reaction (PCR) of the region of interest of the DNA target as well as labeling of the DNA samples by using fluorophores. These steps involve time consuming thermal cycles and sample pre-treatment; in addition they are subject to contamination problems and require expensive reagents. So a mayor challenge for rapid and reliable DNA analysis appears to be the development of methods that are based on label-free detection systems and do not require the polymerase chain reaction (PCR) amplification of the genetic samples

Both these requirements can be satisfied by Surface Plasmon Resonance imaging (SPRi), which is an optical technique used to monitor interactions established between receptors immobilized on a metal surface and analytes which are put in contact with the sensor surface.[2,3,4] One of the main advantage of SPRi is the possibility of working without the use of labels such as fluorescent tags. Since the labelling step involves chemical modification of analytes, there is the risk that the properties and the function of the molecules are altered, especially in the case of biological systems. In addition, labelling imposes extra time and cost demands. Therefore label-free techniques such as SPRi offer preferred approaches for the analysis of biomolecular interactions such as DNA hybridization or antigen–antibody, protein–DNA, protein–protein and enzyme–substrate interactions. Moreover, the technique permits to monitor interactions rapidly and in real time. Unfortunately, the use of SPRi for genomic assays is limited by the reduced

sensitivity in the detection of hybridized DNA or RNA samples. However, a number of different strategies aimed at overcome the lack of sensitivity for unamplified DNA or RNA detection have been recently investigated.[5,6] In particular, the use of properly functionalized colloidal gold nanoparticles (AuNps) have been shown to be useful in achieving a fM sensitivity in DNA target detection.[7,8,9]

The use of peptide nucleic acid (PNA) probes have also been reported to improve both selectivity and sensitivity in targeting complementary DNA and RNA sequences.[10]

Dealing with immobilized probes means that the target/probe interaction depends on passive diffusion of DNA samples toward the sensing probes. The limited solid-liquid diffusion greatly hinders the hybridization rate of target DNA and sensing probe. Thus, the hybridization time for DNA and immobilized-probe normally takes up to several hours and sometimes a large amount of sample. Moreover, washing steps are also normally required after the hybridization process to remove non-specific binding with the sensor surface. This further increases the whole process time. Therefore, it is important to develop DNA detection assays which are automated, even more easy to perform, faster and more accurate. They should imply low sample consumption, multiplex DNA analysis, integration and portable devices realization.

Droplet-based microfluidics contributes to define new and very powerful approaches for biomolecular diagnostics. Since its advent it has drawn great attention for its capability of miniaturizing typical laboratory operations using a fraction of the volume of reagents in significantly less time. Droplet-based microfluidic systems have been shown to be compatible with many chemical and biological reagents. The ability to rapidly create highly uniform aqueous droplets with controlled contents

enables the rapid analysis of very small quantities of reagents in a p ortable, automated and inexpensive format. The control of the separate and different molecular processes established within the droplets requires specific experimental conditions to be identified and optimized. For this reason, efforts have been paid in identifying experimental procedures to be used in content control. Moreover, the understanding of the mechanisms underlying the droplet formation process allowed several capabilities to emerge, like the possibility of droplets to be individually transported, mixed and analyzed.

The purpose of my research activity was the identification of new methodologies useful for DNA and RNA detection with the principal aim to perform the analysis with a very small amount of samples. Two fields were investigated: i) the ultrasensitive DNA detection obtained by using the metallic nanoparticle-enhanced surface plasmon resonance sensing and ii) droplet-based microfluidics.

In particular, the ultrasensitive detection of DNA and RNA was investigated by coupling microfluidic devices with the SPRi apparatus. A similar approach allowed a real time label-free detection of the nucleic acid. The SPRi capability in term of selectivity and sensitivity in the targeting DNA samples was investigated by employing surface-immobilized PNA probes in combination with a gold nanoparticle-enhanced detection. The potential in detecting specific genomic DNA sequences was also investigated. The experiments were carried out by using microfluidic devices, fabricated by replica molding procedures, which allowed multiplexed DNA detection procedures to be identified and optimized.

The study of droplet-based microfluidic procedures for the detection of biomolecular systems started by investigating the possibility to create highly uniform aqueous droplets with carrying controlled amounts of chemical species. The droplet

interface acts as a membrane confining the droplet content and allowing a large number of reactions and molecular processes to be established within such micro-compartment. The control of the separate and different molecular processes established within the droplets required specific experimental conditions to be identified and optimized. For this reason, efforts have been paid in identifying experimental procedures to be used in content control. Moreover, the understanding of the mechanisms underlying the droplet formation process allowed several capabilities to emerge, like the possibility of droplets to be individually transported, mixed or analyzed.

The detection of interaction events in microdroplets were investigated by using labeled biomolecules, such as DNA or PNA beacons, and suitable detectors (such as that present in fluorescence microscopes) with the principal aim to identify new tools to be used in the simple and cheap sensitive detection of biomolecular systems.

2. SURFACE PLASMON RESONANCE OPTICAL DETECTION

Surface plasmon resonance (SPR) is a powerful technique for the high sensitive and label-free detection of a large range of biological interactions occurring on a surface. SPR biosensors have been applied in numerous important fields including medical diagnostics, environmental monitoring, and food safety and security.[11]

The physical phenomenon of SPR was observed for the first time by Wood[12, 13] in 1902 as a pattern of dark bands in the spectrum of the diffracted light, when he illuminated a metallic diffraction grating with polychromatic light on a mirror with a diffraction grating on its surface.

A physical interpretation of the phenomenon was initiated by Lord Rayleigh[14] and further refined by Fano, who concluded that these "anomalies" were associated with the excitation of electromagnetic surface waves on the surface of the diffraction grating.[15] However, only in 1968 a complete explanation of the phenomenon was possible thanks to Otto[16] and in the same year Kretschmann and Raether[17] who reported the excitation of surface plasmons. The pioneering work of Otto, Kretschmann and Raether established a co nvenient method for the excitation of surface plasmons and their investigation, and introduced surface plasmons into modern optics.

In the late 1970s, surface plasmons were first employed for the characterization of thin films[18] and the study of processes at metal boundaries[19], while application of SPR-based sensors to biomolecular interaction monitoring was first demonstrated in 1983 by Liedberg et al.[20] Subsequent efforts in research and development, relied on the combination of three unrelated fields: optics, microfluidics and surface chemistry, resulted in the successful development of the instrumental concept of

biomolecular interaction analysis (BIA). In 1990, Pharmacia Biosensor AB launched the first commercial SPR product, the Biacore instrument.[21]

Surface plasmons (SPs) can be considered as propagating electron density waves occurring at the interface between metal and dielectric.[22]

The free electrons of a metal are treated as an electron liquid of high density of about $10^{23}cm^{-3}$ called "plasma". Electron density fluctuations which propagate through the volume of the metal have characteristic frequency (eq. 1):

$$\hbar\omega_p = h\sqrt{\frac{4\pi ne^2}{m_e}} \qquad \text{eq. 1}$$

where ω_p is the frequency associated to plasmon oscillations, n is the free electron density of the material, e is the electron charge, and m_e is electron mass. When the plasma is excited by an external source with a frequency equal to ω_p, it was shown that the electrons collectively and coherently oscillate in the material.[23] These charge density fluctuations propagating through the metal volume referred to as "bulk plasmons" have an energy in the case of gold of 3.22 eV.

Taking into account a metallic surface interfaced with a medium having a dielectric constant ε_1, the electronic charges on metal boundary can perform coherent fluctuations which are confined at the interface and vanishes both sides of the metal surface. The fluctuations occurring on the surface are called "surface plasmons". This plasmon waves have *p*-character because the surface charge induce the oscillations of the electric field in the surface normal *z*-direction, while *s*-polarized waves have only oscillations of the electric field in the surface parallel x-direction (**Figure 1**). Surface plasmons are described by a wave vector $\boldsymbol{K_{sp}}$ parallel to the *x* direction. Gold surface plasmons have an energy of 2.28 eV. The frequency ω_p of

the surface plasmon longitudinal oscillations is tied to its wave vector $\boldsymbol{K_{sp}}$ by a dispersion relation[24]:

$$\left|\vec{K}_{sp}\right| = \frac{\omega}{c}\sqrt{\frac{\varepsilon_1\varepsilon_2}{\varepsilon_1+\varepsilon_2}} = \frac{2\pi}{\lambda}\sqrt{\frac{\varepsilon_1\varepsilon_2}{\varepsilon_1+\varepsilon_2}} \qquad \text{eq. 2}$$

$\varepsilon_2=\varepsilon'_2+i\varepsilon''_2$ is the complex dielectric constant, where ε'_2 and ε''_2 being the real and imaginary parts of the dielectric function of a metal at the interface with a medium having ε_1 dielectric constant.

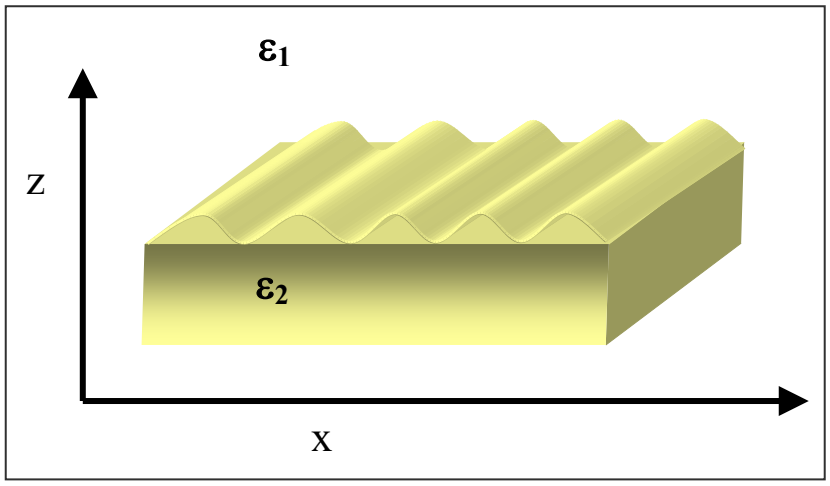

Figure 1: Schematic of surface plasmon waves at the interface between a metal and a dielectric. The plasmon propagates along the x-direction and decays exponentially into the z-direction.

The wave vector of light ($\boldsymbol{K_{light}}$) of the same energy $\hbar\omega_p$ traveling through the medium ε_1 is given by eq. 3

$$\left|\vec{k}_{light}\right| = \frac{\omega}{c}\sqrt{\varepsilon_1} \qquad \text{eq. 3}$$

For surface plasmon excitation by a photon to take place, the wave vector of photon $\boldsymbol{K_{light}}$ and surface plasmons $\boldsymbol{K_{sp}}$ should be equal in magnitude and direction for the same frequency of the waves.

We can obtain a graphical representation of SPR dispersion relation as shown in **Figure 2**.

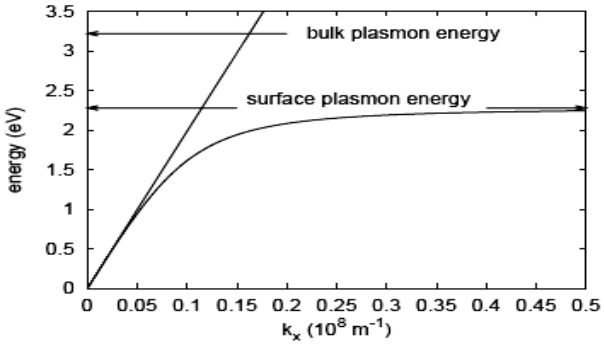

Figure 2: Surface plasmon dispersion ω(kx) on gold surface. The vertical axis is scaled as ħω (eV). The straight solid line in the figure shows the light line kx = $\sqrt{\epsilon_2}\omega/c$. The energy of bulk plasmon is 3.22 eV, and that of surface plasmon is 2.28 eV and shown as the arrows in the figure.

We can see that, apart from the origin, there is no point where the SPR curve and the light curve intersect. As a consequence, in this geometry a freely propagating beam of light incident upon the metal surface cannot excite a surface plasmon.

$$\frac{\omega}{c}\sqrt{\varepsilon_1} \neq \frac{\omega}{c}\sqrt{\frac{\varepsilon_1 \varepsilon_2}{\varepsilon_1 + \varepsilon_2}} \qquad \text{eq. 4}$$

Therefore, SPs are "nonradiative" fluctuations of the surface electron density since they cannot couple to wave light in a simple way: the SPs excitation with light needs special light-plasmon couplers.

One way to circumvent this problem is the use of a metal layer on which a periodic structure is prepared[25] as illustrated in **Figure 3**.

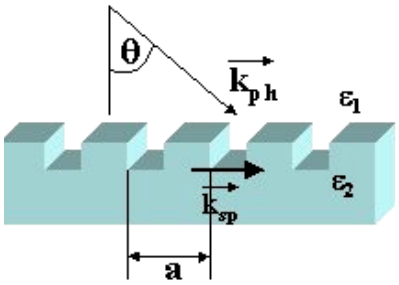

Figure 3: Scheme of a diffraction grating

When light falls on such a structure, this acts as a diffraction grating. Diffraction gives rise to a series of diffracted waves. If light hits a grating with a periodicity *a*, at a θ angle, the component of the generated wave vector in the plane of the grating can be written as:

$$\left|\vec{K}_{ph}\right| = \frac{\omega}{c} n_2 \sin\theta + m\frac{2\pi}{a} \qquad \text{eq. 5}$$

where m denotes the diffraction order. For a given angle of incidence θ, the matching condition for resonance can be fulfilled when

$$\frac{\omega}{c} n_2 \sin\theta + m\frac{2\pi}{a} = \frac{\omega}{c}\sqrt{\frac{\varepsilon_1\varepsilon_2}{\varepsilon_1+\varepsilon_2}} \qquad \text{eq. 6}$$

The disadvantage of grating-based sensors is that the light beam is incident through the sample solution, which may give some inaccuracies if the sample is absorptive.

Another way of providing a wave vector appropriate for SP excitation is by means of a prism couple and the attenuated total reflection (ATR) method. There are two configurations of the ATR method: Kretschmann geometry and Otto geometry.

In the Kretschmann geometry of the ATR method [26] (**Figure 4**), a high refractive index prism with a refractive index n_{pr} is interfaced with a metal-dielectric waveguide consisting of a thin metal film with dielectric constant ε_2 and a dielectric with a refractive index n_1 ($n_1 < n_{pr}$).

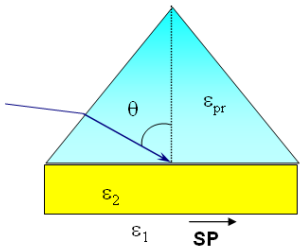

Figure 4: Configuration of Kretschmann geometry

When p-polarized light hits on the prism side opposite to the thin metal, at θ angles greater than the critical one obtained from the Snell's law:

$$\sin\theta = \frac{\varepsilon_1}{\varepsilon_{pr}} \qquad \text{eq. 7}$$

light will be totally internally reflected and an evanescent field is generated at the point of internal reflection. The wave vector of the incident radiation takes the form:

$$\left|\vec{k}_{pr}\right| = \frac{\omega}{c}\sqrt{\varepsilon_{pr}}\,sen\,\vartheta \qquad \text{eq.8}$$

At a certain angle of incidence, the wave vector of the incident light matches the SP wave vector and the coupling condition is satisfied:

$$\frac{\omega}{c}\sqrt{\varepsilon_{pr}}\,\sin\theta = \frac{\omega}{c}\sqrt{\frac{\varepsilon_1\varepsilon_2}{\varepsilon_1+\varepsilon_2}} \qquad \text{eq. 9}$$

The coupling of the field and the free surface electrons is evidenced by a drop in intensity of reflected light[27] (**Figure 5**).

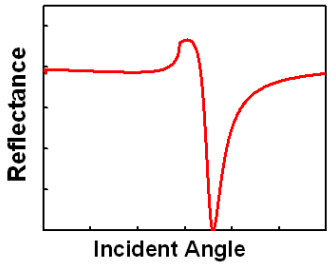

Figure 5. Attenuated total reflection (ATR).

Charge density fluctuations induced by the photons/plasmons matching will also be p-polarized and will enhance the evanescent electric field amplitude which penetrates into the medium ε_1. SPR sensors investigate only a very limited vicinity or fixed volume at the metal surface. The penetration depth of the electromagnetic field (so-called evanescent field) at which a signal is observed typically does not exceed a few hundred nanometers, decaying exponentially from the surface in the direction perpendicular to the metal-dielectric interface with a distance within which the field intensity decreases by a factor of 1/e. The penetration depth depends on the wavelength and is given by $\mathbf{(1/2k''_x)^{-1}}$ where $\mathbf{k''_x}$ is imaginary part of wave vector to the metal-dielectric interface.[28]

Considering that coupling conditions are depending from the dielectric constants of all the involved media including the prism, the metal layer and the dielectric medium in contact to the metal surface, any variation of the dielectric constant value of the region at the interface with the gold layer, within the range of penetration of the evanescent field, causes a variation into the parameters that fulfill the matching condition (eq. 9) and so, a shift in in the resonance angle.[29] Such a distinguishing property is the basic principle which makes the surface plasmon resonance useful as biosensor.[30]

In the Otto geometry (**Figure 6**), a light a high refractive index (n_{pr}) prism is interfaced with a dielectric-metal waveguide consisting of a thin dielectric film with refractive index n_1 ($n_1<n_{pr}$) and a semi-infinite metal with dielectric constant ε_2.

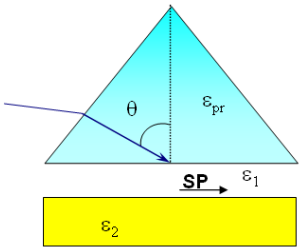

Figure 6. Excitation of surface plasmons in the Otto geometry of the ATR method.

According to this geometry, a light wave incident on the prism-dielectric film interface at an angle of incidence larger than the critical angle for these two media produces an evanescent wave propagating along the interface between the prism and the dielectric film. If the thickness of the dielectric layer is chosen properly (typically few microns), the evanescent wave and a surface plasmon at the dielectric-metal interface can couple.

Conditions for surface plasmon resonance are obtained in the infrared and visible wavelength region for air/metal and water/metal interfaces. Metals that support surface plasmons are silver, gold, copper, aluminum, sodium, and indium. The key parameters for the choice of a metal for SPR are: *i*) the purity of the surface: oxides and sulfides formed after the metal interaction with the atmospheric can interfere with SPR phenomenon; *ii*) compatibility of the metal reactivity with the surface chemistry needed for the realization of SPR experiments. Among several metals, gold is the most commonly used because it resists to oxidation, produces a strong SPR effect in the near-infrared region and is suitable for a convenient surface

chemistry useful for the immobilization of a v ariety of chemical and biological species.

Typically, an SPR sensor surface (**Figure 7**) is composed by gold (45 nm) deposited onto a glass slide with a chromium adhesion layer (5 nm).[31]

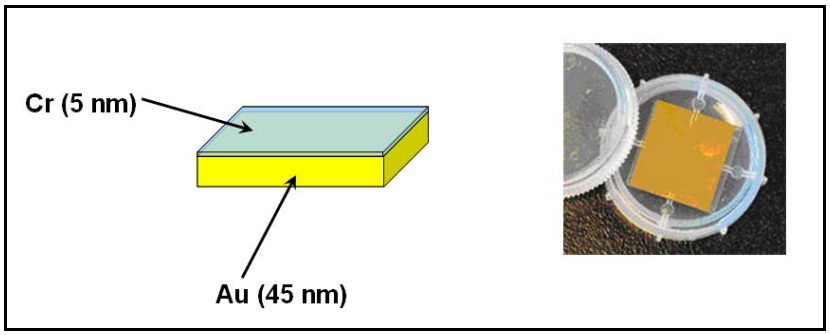

Figure 7. Typical SPR sensor.

A surface plasmon resonance biosensor is able to measure the binding between target analyte molecules and a receptor immobilized on the gold surface. During the receptor/analyte binding event the shift of the dip in the spectrum of reflected light (modulating λ or θ) is monitored over time as SPR signal, and association, dissociation, kinetic information regarding biomolecules are gathered. SPR has the potential to investigate interactions between antigen/antibody couple, DNA-probe and its complementary strand, substrates and enzymes.[32] SPR requires no labeling of the interacting components; the time required for the analysis is typically in the range of a few minutes; the sample consumption is in the nanomole-picomole range. The kinetic events at the metal surface, displayed as a *sensorgram*, can be investigated by monitoring the SPR signal change as a function of time. The time interval during which the analyte interacts with the surface bound receptor defines the 'association phase' whereas the time interval following the analyte interaction is termed 'dissociation phase'. In the association phase there is a simultaneous association and dissociation equilibrium. A steady-state condition is reached when the association

rate equals the dissociation rate. Under ideal experimental conditions, only dissociation should take place during the dissociation phase.

In order to perform replicate SPR experiments any bound analyte molecule should be removed with no disrupting of the receptor structure and activity. So, a typical SPR experiment involves several steps displayed in **Figure 8**. Each measurement starts with conditioning the sensor surface with a suitable buffer solution (equilibration). It is of vital relevance to have a reliable baseline before the capturing event starts. At this point, the sensor surface contains the active ligands, ready to capture the target analytes. On injecting the solution containing the analytes, they are captured on the surface (association). Also other components of the sample might adhere to the sensor surface; without a suitable selection of the ligand, this adherence will be non-specific, and thus easy to break. At this step, adsorption kinetics of the analyte molecule can be determined in a real-time measurement. Next, buffer is injected on to the sensor and the non-specifically bound components are flushed off. In this step, dissociation of the analyte starts, enabling the kinetics of the dissociation process to be studied.

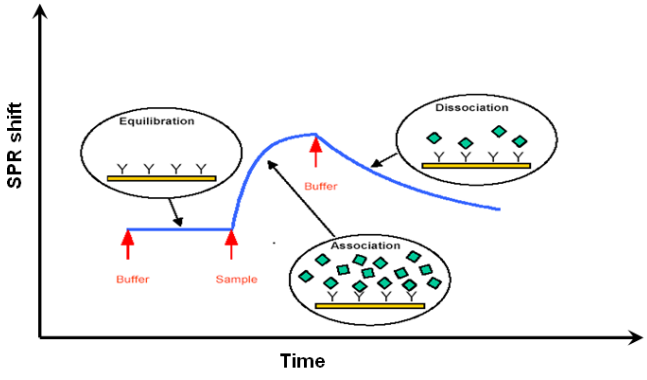

Figure 8: Sensorgram for receptor-analyte interaction

Finally, a regeneration solution is injected, which breaks the specific binding between analyte and ligand (**Figure 9**). If properly anchored to the sensor surface,

the ligands remain on the sensor, whereas the target analytes are quantitatively removed (ideal condition). It is vital in order to perform multiple tests with the same sensor chip to use a regeneration solution which leaves the activity of the ligands intact, as the analysis cycle is required to take place repeatedly for hundreds, sometimes even thousands of times. Again, buffer is injected to condition the surface for the next analysis cycle. If the regeneration is incomplete, remaining accumulated mass causes the baseline level to be increased.

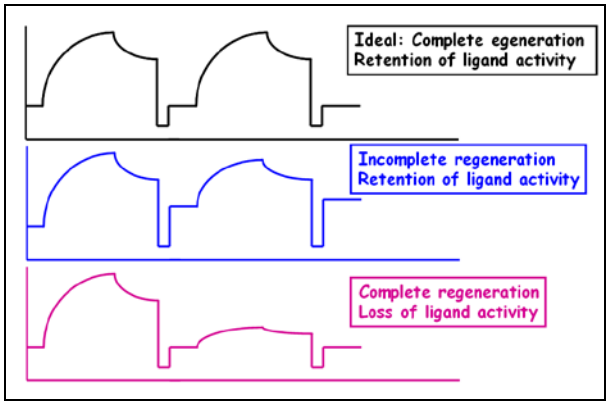

Figure 9. Regeneration.

It is worth to notice that the change in the refractive index produced by the capture of biomolecules depends on the concentration of the analyte molecules at the sensor surface. If the binding occurs within a layer of thickness *h*, the SPR response is proportional to the binding induced refractive index change, which can be expressed as:

$$\Delta n = \left(\frac{dn}{dc}\right)\frac{\Gamma}{h} \qquad \text{eq. 10}$$

where (*dn/dc*) denotes the refractive index increment of the analyte molecules and **Γ** denotes the surface concentration in mass/area. Consequently, quantitative measurements of biomolecules adsorption can be obtained with SPR technique.[33]

SPR measurements can be carried out to determine the kinetics of a binding process, since the monitoring of SPR signal allows to estimate the association (k_a) and dissociation (k_d) rate constants of the analyte-receptor interaction.

$$A + B \underset{k_d}{\overset{k_a}{\rightleftharpoons}} AB$$

The affinity of the interaction can be described as "association constant" or affinity constant K_A given by the ratio of the k_a and k_d. The affinity can be also expressed as "dissociation constant" or K_D, which is simply the inverse of the K_A.

The SPR data are analyzed through the use of modeling of interactions[34] and fitting experimental data.[35] The choice of a kinetic model should be based on the understanding of the underlying chemistry or physiology. For a general reaction between a surface immobilized receptor (A) and an analyte (B) that interact according to a simple bimolecular association (Langmuir binding) a first order kinetic can be assumed.[36]

The differential rate equation describes the relation between the parameters:

$$\frac{d[AB]}{dt} = k_a [A][B] - k_d [AB] \qquad \text{eq. 11}$$

The SPR response (R) is proportional to the amount of the [AB] receptor-analyte complex concentration onto the metallic surface; while maximum SPR signal (R_{max}) produced when all the surface binding sites are occupied is proportional to initial concentration of [A] onto the surface. So, eq. 11 can be rewritten as:

$$\frac{dR}{dt} = k_a [B](R_{\max} - R) - k_d R \qquad \text{eq. 12}$$

or:

$$\frac{dR}{dt} = k_a [B] R_{\max} - (k_a [B] + k_d) R \qquad \text{eq. 13}$$

k_a and k_d values can be obtained from the equations 12-13 by linearization,[37] curve fitting with analytical integration, or curve fitting with numerical integration.[38]

Linearization can be obtained by taking into account, from eq. 13, only the association phase; a plot of dR/dt versus R will therefore have a slope

$$(-k_s) = - (k_a[B]+k_d) \quad \text{eq. 14}$$

Straight lines were fit to the initial linear portion of the transformed association phase to obtain k_s. These values are plotted against concentration of [B] and the slope of this second line is k_a.

During the dissociation phase [B] = 0, so from eq. 13 we obtain:

$$\frac{dR}{dt} = -k_d R \qquad \text{eq. 15}$$

The integration of eq. 15 gives:

$$R = R_0 e^{-k_d t} \qquad \text{eq. 16}$$

k_d is calculated from the slope of the curve obtained by plotting ln (R_0/R) versus time.

Analysis by linearization or integrated rate equation is adequate for interpreting simple bimolecular interactions. Integration of the differential rate equation for a simple bimolecular interaction (Eq.13) yields eq. 17:

$$R = k_a [B] R_{\max} \left[1 - e^{-(([B]k_a + k_d)t)}\right] \Big/ ([B]k_a + k_d) \qquad \text{eq. 17}$$

However, many interactions studied by SPR do not fit the simply bimolecular model. The numerical integration of the differential rate equation can be used to

obtain the final rate equation and the rate constants can be derived by non linear regression based on the so obtained rate equation. Numerical integration can be used to model any kinetic mechanism and in order to minimize mistakes, the data are usually analyzed globally by fitting both the association and dissociation phases for several concentrations simultaneously. This means that several related curves are fitted simultaneously giving one and more robust answer for the rate constants.[39]

SPR measurements can be made in a variety of formats that are classified according to the method used to detect the light wave modulated by surface plasmons. Traditional instruments are used for scanning-angle experiments, in which the change in percent reflectivity is measured as a function of incident angle, while the wavelength of light is held fixed. This SPR method has been popularized by the commercially available BIAcore instrument (www.biacore.com). Another common method is FT-SPR, which is based on the scanning of light wavelength as the angle of incidence is held fixed.[40]

One of the main advantage of SPR is the possibility of working without the use of labels such as fluorescent tags. Most screens that are used in drug discovery require some type of fluorescent labelling or radiolabelling to report the binding of a ligand to its receptor. Since the labelling step involves chemical modification of analytes, there is the risk that the properties and the function of the molecules are altered, especially in the case of biological systems. In addition, labelling imposes extra time and cost demands and can in some cases interfere with the molecular interaction by occluding a binding site, which leads to false negatives, or producing a background binding, leading to false positives. Therefore label-free techniques such as SPR offer preferred approaches for the analysis of biomolecular interactions, which constitute a key part of the drug discovery process, such as DNA hybridization

or antigen–antibody, protein–DNA, protein–protein and enzyme–substrate interactions.[41,42] Moreover, the technique permits to monitor interactions rapidly and in real time.

In contrast to traditional SPR techniques, SPR imaging(SPRI), also called SPR microscopy, is performed with both the wavelength and the angle of incident light fixed, measuring the change in the reflected light intensity across the surface where an array of molecules is present. SPRI combines the advantages offered by the traditional SPR in term of real time analysis, no labeling requirements and high sensitivity, with those associated to an imaging system such as the simultaneous monitoring of the interaction of biomolecules arrayed onto the metal surface and the possible coupling with microfluidic devices.[43,44]

Surface Plasmon Resonance Imaging[2, 45] was introduced by Rothenhäusler and Knoll[46] in the 1988. Since then SPRI has been proposed as a powerful analytical technique able to investigate interactions between (macro)molecules and/or biomolecules arrayed onto chemically modified gold surfaces.[47]

In an SPRI experiment, spatial differences in percent reflectivity Δ%R (which can be seen as brighter or darker regions in the SPR image) are measured at a fixed angle and wavelength. A collimated p-polarized beam of light is used to illuminate a prism/thin gold film sample assembly at a single incident angle (near the SPR angle) and the intensity of the light reflected from the gold surface is detected with a charge coupled device (CCD) camera to produce the SPR image. The surface functionalization with a spatially controlled pattern of specific binding sites allows to observe in real time how the reflectivity minimum shifts depending on the adsorption processes occurring at these surface areas modified in spatially resolved manner. The spatial contrast in an SPR image comes from the heterogeneity in the complex

dielectric due to differences in refractive index or film thickness near the surface at different positions across the surface, which results in slight shifts in the resonance angle. If an adsorbate has a refractive index different from that of the solvent, its presence on the surface can be detected with spatially resolution by monitoring changes in the reflected light intensity. Difference images obtained by the subtraction of a reference image from a post-binding image provide visual confirmation of the binding events: where binding occurs, reflectivity increases and regions of interest become brighter.

SPR imaging technology can be used to screen a variety of ligands for a particular protein of interest, thus facilitating the analysis of the protein's functions in biological systems.[48] Recently, potentials of SPR imaging for the detection of DNA:DNA, RNA:DNA, and DNA-protein have been demonstrated.[49,50,51] However the use of SPRI for genomic assays is limited by the reduced sensitivity in the detection of hybridized DNA or RNA samples. Thus, a number of different strategies aimed at amplifying the SPRI response to DNA and RNA hybridization have been recently investigated,[52,53] in particular using colloidal gold nanoparticles (AuNPs).[54,55]

On the other hand, another aspect which deserves attention is the sequence-specificity, in particular when single nucleotide polymorphisms (SNPs) or point mutations are concerned.[56,57,58] SNPs can be involved in genetic diseases and increase the risk of cancer, but they could also be used as genetic markers to study and understand the human evolution. Many methods have been dedicated to the detection of DNA mutations due to their biological and medical impacts. In this perspective, interesting results were obtained by combining SPRI biosensing to the peptide nucleic acids (PNA) in targeting complementary DNA sequences.[59]

3. PEPTIDE NUCLEIC ACID (PNA)

PNA is an synthetic DNA mimic, introduced by Nielsen et al. in 1991,[60] in which the negatively charged phosphate deoxyribose backbone is replaced by repeating neutral N-(2-aminoethyl)-glycine units linked by peptide bonds and the various purine and pyrimidine bases are linked to the backbone by methylene carbonyl bonds (**Figure 10**). PNAs have been shown to efficiently hybridize complementary DNA and RNA sequences with improved selectivity and sensitivity than DNA. Enhanced PNA targeting capabilities are related by the stronger interaction with the complementary DNA stand in comparison to the corresponding DNA/DNA interaction, caused by the absence of charges on the PNA backbone. In fact, the neutrality of the backbone prevents any electrostatic repulsion of the complementary DNA strand. PNAs offer a variety of other advantageous features with respect to DNA such as: *i*) superior pair mismatch discrimination; *ii*) reduced needs for high-salt condition to obtain hybridization; *iii*) better thermal stability of the PNA:DNA duplexes compared to the DNA:DNA equivalents; *iv*) stability over a wide pH range. PNAs are also resistant to enzyme degradation since they are not easily recognized by nucleases and proteases.

The thermal stability of the PNA/DNA duplexes is strongly affected by the presence of imperfect matches. Such presence of mismatches in a PNA/DNA duplex is much more destabilizing than a mismatch in a DNA:DNA duplex. This property of PNA is responsible for the remarkable discrimination between perfectly matching and mismatching sequences offered by PNA probes, and makes them so attractive as DNA recognition elements in biosensor technology. Since PNAs have been shown to be able to improve both selectivity and sensitivity in targeting complementary DNA

and RNA sequences, [10, 61] they have been proposed as valuable alternatives to oligonucleotide probes.[62]

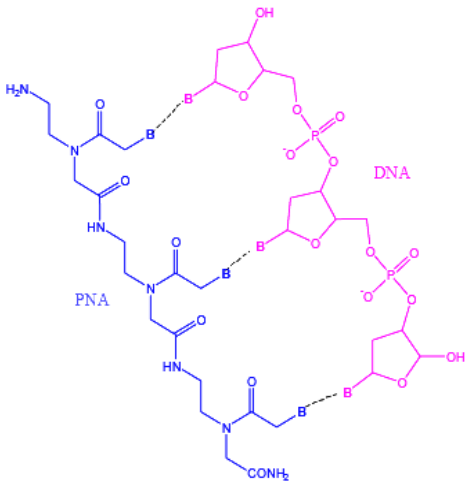

Figure 10. Structures of double strand of PNA and DNA hybridization.

Surface plasmon optical detection of PNA/DNA and PNA/RNA hybridization was demonstrated since the end of 1990s. At that time efforts were paid in demonstrating the advantages offered by the use of PNA in DNA recognition. In this perspective, the effects on the SPR detection of the improved stability of the complex formed after the DNA or RNA detection were investigated. In order to compare the stability of PNA/DNA and DNA/DNA hybrids, biotinylated 21-mer oligonucleotide were immobilized on a streptavidin-coated sensor chip and then the interaction with the complementary PNA or DNA 9-mer molecules were evaluated by using an SPR based biosensor.[63] An increased SPR response was detected for the PNA/DNA hybridization. A specific study of the kinetics of the dissociation processes revealed that the PNA/DNA hybrids are much more stable than DNA/DNA hybrids. Nevertheless, when longer PNA and DNA probes were used (14-mers), both PNA/DNA and DNA/DNA hybrids showed similar stability.

The thermal stabilities and the kinetics of the PNA/DNA, PNA/PNA and PNA/RNA reactions were also quantitatively evaluated by immobilizing PNA sequences on the SPR sensor surface. In particular, changes in the SPR response were compared when oligonucleotides, which were either fully matched to the immobilized PNA or contained mismatched bases, were absorbed on the PNA immobilized surfaces.[64] The introduction of a single mismatch at the centre of pentadecamer PNA/DNA and PNA/RNA duplexes brings about increased dissociation and decreased association rate constants. The comparison of melting temperatures (T_m) for full-match and single mismatch sequences shows that T_m values are generally 4°C higher for PNA/RNA duplexes than those measured for the corresponding PNA/DNA duplexes. In accordance with the observed thermal stabilities, higher association and lower dissociation rate constants were found for PNA/RNA duplexes compared to PNA/DNA duplexes. It is worth noting that the fully complementary PNA/PNA duplexes showed higher T_m and k_a and lower k_d values in comparison to the values obtained from the corresponding PNA/DNA and PNA/RNA duplexes. These report showed the first systematic study of the effects of the presence of mismatches on the kinetics of the hybridization processes involving PNA oligomers

The use of surface-immobilized PNA probes in SPR detection provides a powerful tool for the study of pathogenic DNA. Unfortunately, limitations arise from the reduced sensitivity in the SPR detection of hybridized DNA or RNA samples. Convenient detection limits have been obtained by PCR amplifying the DNA target or by culturing the organism possessing the pathologic DNA before the SPR analysis. PCR-based amplification produces double-stranded DNA molecules that are detected by PNA probes because of the strong bind to the DNA complementary

strand. Indeed, it was demonstrated that binding to 'Watson–Crick complementary' target in double-stranded DNA by PNA takes place via strand displacement as a consequence of the extraordinarily high stability of the PNA/DNA complex.[65,66] In particular, the specific detection of PCR-amplified pathogen DNA encoding verotoxin 2 extracted from *Escherichia coli* O157:H7 was investigated by using both DNA and PNA probes.[67] As expected, the DNA probe generated a s maller SPR signal confirming that PNA/DNA duplexes are more stable than DNA/DNA duplexes. A detection limit of 7.5 pmol was obtained in the detection of the analyte PCR products. Moreover, it was demonstrated the possibility of detecting pathogenic DNA from stool samples and spiked stool samples. A similar approach was used for the detection of PCR products containing the Shiga toxin-2 (stx-2) genes in stool samples spiked with *E. coli* O157:H7 and in fecal samples from patients and healthy carriers.[68]

The immobilization of the PNA probe is an essential step in the development of a whole range of biosensors. In particular, SPR data reproducibility, sensitivity and selectivity are affected by lacks in the surface probe immobilization procedures.

The biotin-streptavidin coupling reaction is typically used for the immobilization of biotinylated nucleic acid probes. Streptavidin (like avidin) is a tetrameric protein with an exceptionally high affinity to biotin.[69] The effect of the PNA probe immobilization through biotin-streptavidin coupling reaction on the binding capacity of the sensor surface has been studied.[70] In particular, the hybridization efficiencies of a P NA probe immobilized on an SPR sensor surface through covalent or biotin-streptavidin coupling reaction were compared. The covalent binding approach was carried out by using a carboxylated dextran matrix activated with *N*-hydroxysuccinimide (NHS) and 1-ethyl-3-(3dimethylaminopropyl)-

carbodiimide (EDC) and thiolated by addition of cystamine dihydrochloride followed by reduction with 1,4-dithioerythrite (DTE). The PNA probe, modified at its N-terminal with a maleimide group, was coupled to the sulfhydryl groups of the modified dextran matrix. Immobilization by covalent attachment has proven to be superior in stability, compared to non-covalent immobilization. In fact, ssDNA hybridization to PNA probes covalently bound to the dextran surface showed small signal loss from one measurement to another while decreased SPR signal intensities were revealed from sensors based on biotin-streptavidin probe immobilization. The SPR signal modification was a consequence of a decreased capacity of the surface for hybridization caused by the progressive loss of probe. A new immobilization of the probe restored the surface binding capacity. It was noted that since biotin-streptavidin binding is based on non-covalent interactions, the application of harsh conditions (e.g., regeneration of the surface with NaOH) destabilizes the PNA/DNA complex leading to PNA probe loss.

4. MICROFLUIDICS

Microfluidics is defined as the science and technology of systems that process or manipulate small (from nanolitres down to attolitres) amounts of fluids, using channels with dimensions of tens to hundreds of micrometres.[71] Since its advent, microfluidics has drawn great attention for its capability of miniaturizing typical laboratory operations using a fraction of the volume of reagents in significantly less time.

Compared with the macroscale, microfluidic systems offer significant advantages such as short times for analysis, improvements in mass and thermal transfer, reduced sample volume, potential of automation and integration (lab-on-a-chip, micro Total Analysis Systems μTAS). Thanks to its small size and the laminar flow of fluids in microchannels, microfluidics offers fundamentally new capabilities in the control of concentrations of molecules in space and time.

The design of a microfluidic device often requires the assembly of several components, such as a system for the introduction of reagents, systems to move and mix fluids inside the chip, including valves, mixers and pumps, capable of controlling fluid flow by utilizing the physics of the microscale and various other components (such as detectors and systems for purification of products. This design often requires unusual geometries and the interplay of multiple physical effects that lead to interesting variants of well-studied physical properties of fluids moving in large channels and some new fluid responses.[72]

One of the most important phenomenon that differentiates macroscopic and microfluidic systems is turbulence. On large scales, fluids mix convectively, reflecting the fact that in macroscopic fluids inertia is often more important than viscosity. On the contrary, in micrometre-scale channels fluids do not mix

convectively but they flow in parallel, without eddies or turbulence; the only mixing that occurs is the result of diffusion of molecules across the interface (laminar flow) and specific components are required to obtain mixing.

Droplet-based microfluidic systems, unlike continuous flow systems, create discrete small volumes using immiscible fluids that are driven into separate microchannels via an independently controlled flow. Typically an aqueous solution is used as a dispersed phase while oil acts as a continuous phase. Reagents are confined in the droplets and each droplet is isolated from the channel walls by the immiscible liquid, thus greatly reducing sample contamination and eliminating reagent dispersion problems. Moreover, each droplet can be considered as an isolated microreactor and each microreactor can be individually controlled and analyzed.[73,,74] This allows parallel processing, higher throughput and less sample consumption than continuous flow systems. Furthermore rapid mixing of reagents inside the droplets can be achieved: the rate of DNA hybridization in an homogeneous solution is about 40-fold faster than the hybridization rate in solid-liquid interfaces such as those of microarrays.

Droplets and particles have the potential to become important tools for drug delivery and biosensing. However, in order to properly use them correct dosing and manufacturing must be ensured. Since biological and chemical properties of microparticles are strongly affected by both their size and morphology, it is essential to be able to generate these structures at well-defined volumes and composition.[75] The majority of microfluidic methods produce droplet diameters ranging from a few micrometres to hundreds of micrometres. Polydispersity, defined as the standard deviation of the size distribution divided by the mean droplet size, can be 1–3% while droplet volumes range from femtolitres to nanolitres. [76]

Factors such as the use of surfactants, the viscosity of the immiscible phases, and the wettability of the channel walls can be used to manage the size of the formed droplets. The hydrophilicity or hydrophobicity of the microchannel surface also determines which liquid phase is dispersed.

Droplet-based microfluidic systems have been shown to be compatible with many chemical and biological reagents. The ability to rapidly create highly uniform aqueous droplets with controlled contents enables the rapid analysis of very small quantities of reagents in a portable, automated and inexpensive format. In addition, it is possible to split the single droplet into two or more droplets or keeping reagents separate until the proper conditions are available and then performing controlled coalescence of droplets. Both droplet fission and fusion can enhance the experimental capacity. These new capabilities have allowed the development of numerous biotechnology applications in the field of protein crystallization, advanced flow cytometry, enzyme kinetics studies, and DNA and blood analysis. [77, 78]

4.1 Droplet generation

Droplets can be generated either by passive or active methods. Passive methods exploit the flow field to deform the liquid interface and to promote the natural growth of interfacial instabilities, avoiding moving parts and explicit external actuation. They can be grouped into three categories, characterized by the nature of the local flow field used to break the droplets: co-flowing streams, cross-flowing streams and elongation-dominated flows (**Figure 11**). In all cases, the continuous phase liquid preferentially wets the walls of closed microchannels and the droplet is prevented from contacting the wall due to an ever-present thin film of the surrounding liquid.

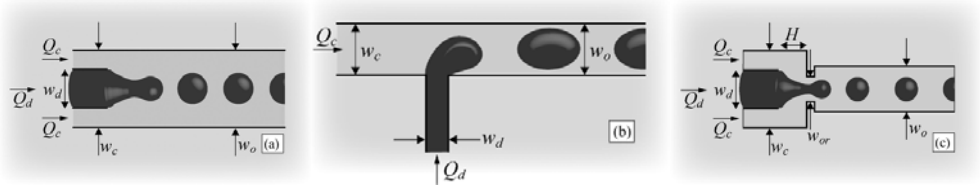

Figure 11. Illustrations of the three main microfluidic geometries used for droplet formation. (*a*) Co-flowing streams, (*b*) crossflowing streams in a T-shaped junction, and (*c*) elongational flow in a flow focusing geometry. *w*d and *w*c are the widths of the two inlet streams. The subscripts 'd' and 'c' indicate the dispersed phase liquid and the continuous phase liquid, respectively. The width of the outlet channel *w*o into which the droplets travel after they break is also indicated. *Q*d and *Q*c, represent the volumetric flow rates. It is assumed that the device is planar with a uniform depth *h*.

In general, the fluid phase to be dispersed and a second immiscible liquid are driven into separate microchannels via independently controlled pressure-driven flows in which either volume flow rate or applied pressure are controlled. The two streams meet at a junction, at which the dispersed phase liquid extends to form a 'finger' or 'jet'. The local flow field, which deforms the interface, is determined by the geometry of the junction and the volumetric flow rates of the two fluids. Finally, a free surface instability leads to the breakup of a droplet from the dispersed phase finger.

The size of the channels and of the orifice where the dispersed phase merges into the continuous phase certainly influences the size of the droplets. Fluids viscosity and surface tension as well as use of surfactants play a key role. [79]

The wettability of nearby channel walls is critically important to the process, determining which liquid phase is dispersed. Controlling wetting of the channel walls by the continuous phase is important when switching between the generation of W/O and O/W emulsions or for the formation of double emulsions. To prevent the discrete phase from adhering to the channel walls, W/O droplets are formed in hydrophobic channels, whereas O/W emulsions require hydrophilic channels. Hydrophobic

treatments such as silanization and siliconization are used to make a hydrophilic surface hydrophobic.[80] Surface treatments such as oxygen plasma and polyvinyl acetate (PVA) coating can be implemented to temporarily convert the naturally hydrophobic surface of PDMS into a hydrophilic surface.[81] Channel coating with PEG has also been used as a hydrophilic surface treatment and a means to prevent protein adsorption.[82]

T-junction is the simplest configuration to form droplets (see **Figure 11b**). The inlet channel containing the aqueous phase perpendicularly intersects the main channel where the continuous phase flows, forming an interface at the junction.[83, 84] The shear forces generated by the continuous phase and the pressure gradient force the dispersed phase to elongate along the main channel until the neck of this same phase thins and eventually breaks to form a droplet. Droplet size can be changed by altering fluid flow rates, channel dimensions or fluid properties such as viscosity between the two phases.

In the flow-focusing configuration,[85, 86] both phases are forced through a narrow region in the microfluidic system (**Figure 11c**). Generation of droplets is more controlled and stable in this case because the design employs symmetric shearing by the continuous phase on the discrete phase. The same parameters listed for the T-junction design govern droplet generation in flow-focusing designs.

In addition to T-junction and flow-focusing methods that depend on channel geometry to control the generation of droplets, emerging technologies have enabled electrodes to be integrated into microdevices to provide electrical control over droplet formation. Two examples of these electrohydrodynamic (EHD) methods are dielectrophoresis (DEP), that generates uniform droplets by pulling them away from a fluid reservoir simply applying a non-uniform electric field,[87, 88] and

electrowetting on dielectric (EWOD), in which droplets are formed by applying an electric field that changes the interfacial energy and so the contact angle between a fluid and the surface it is in contact with.[89, 90]

4.2 Physics at the micrometer scale

In general, relevant fluid properties are viscosity (μ), density (ρ) and interfacial tension (γ). Liquids are typically Newtonian, thus the shear stress is directly proportional to the strain rate within the fluid.

Pressure-driven flow is accomplished using either syringe pumps, which impose constant volumetric flow rates, or gas pressure cylinders, in which a regulator controls the imposed pressures.

At the microscale, different forces become dominant over those experienced in everyday life.[91] Microfluidics has been able to exploit such fundamental differences between fluids flowing at the macroscale and those travelling though microchannels, allowing to perform techniques and experiments not possible on the macroscale and new functionality and experimental paradigms to emerge.[92,] The effects that become dominant in microfluidics include laminar flow, diffusion, fluidic resistance, surface area to volume ratio and surface tension.

The essential fluid physics of a system is in the end dictated by a competition between various phenomena, which could be described by a group of dimensionless numbers expressing their relative importance. Dimensionless parameters define units such as volume, column length, linear flow rate, retention time and pressure drop in terms of quantities that can be assumed to be constant over the entire system. [93]

The Reynolds number, Re, is a particularly useful dimensionless parameter (eq. 18). It describes the relative importance of inertial forces ($U \cdot \rho$, where U is the

average velocity and ρ the fluid density) to viscous forces (μ/L, where μ is the dynamic viscosity and L the characteristic length, such as the diameter of the channel). It can be an indication of tendency of a fluid to move in laminar or turbulent flow conditions.[94]

$$\mathrm{Re} = \frac{\rho U L}{\mu} \approx \frac{Inertial\ Forces}{Viscous\ Forces} \qquad \text{eq. 18}$$

Reducing the characteristic length scale has the same effect on fluid behavior in terms of *Re* as increasing the viscosity of the solution. Quantitatively, for a flow in a circular pipe, a *Re* of ~2300 marks roughly the transition from laminar to turbulent flow. In most microfluidic systems, flows are well below a *Re* of ten and often even below unity, so viscous forces typically overwhelm inertial forces and fluids adopt laminar flow. This fact has important implications and forms the basis of many microfluidics-based technologies but, depending on the particular application, this feature can also pose significant challenges.

In the everyday high-Re macroscopic world, random eddies continuously stretch and fold fluid elements chaotically. As a result of this turbulent mixing, gradients are significantly enhanced and time scales for mixing are dramatically reduced. One of the consequences of laminar flow in the low-Re world of microfluidics, however, is that mixing of molecules in the fluid occurs solely through molecular diffusion, which can result in long mixing times. Purely diffusive mixing can be desirable for some applications but also to be avoided in others. Microfluidic chemical reactors require different solutions to be brought together and mixed rapidly. However, in sorting and analysing the products of reactions, the faster the mixing the harder the separation.

The diffusion time τ_D required for a molecule to diffuse a given distance L scales quadratically with the distance, and can be described the eq. 19:

$$\tau_D = L^2 / 2D \qquad \text{eq. 19}$$

where D is the diffusion coefficient of the molecule ($m^2\ s^{-1}$). During this time, the front of a fluid will have moved a certain distance

$$Z \approx \frac{UL^2}{D} \qquad \text{eq. 20}$$

down the channel. So that the number of channel widths required for complete mixing would be of order: [95]

$$\frac{Z}{L} \approx \frac{UL}{D} = Pe \approx \frac{Convection}{Diffusion} \qquad \text{eq. 21}$$

that is the Peclet number (*Pe*) which expresses the relative importance of convection to diffusion. Microfluidic systems where low *Re* number are encountered, are also often characterized by low Péclet numbers, that is diffusion prevails over convection.

Dealing with immiscible fluids means indeed that there is an interface to take into account. When an aqueous flow encounters an oil flow, competing stresses drive the interface: surface tension acts to reduce the interfacial area and viscous stresses act to extend and drag the interface downstream. These stresses destabilize the interface and cause droplet generation.[84, 96]

Another dimensionless number, the Capillary number (*Ca*), is often used to describe such systems where surface tension plays a central role.

$$Ca = \frac{\mu U}{\gamma} \qquad \text{eq. 22}$$

Where

U = velocity

μ = viscosity

γ= surface tension

When shear is used at high values of Ca, the diameter of the droplets R (m) is then described by the eq. 23:[97]

$$R \approx \frac{\gamma h}{\mu U} = \frac{h}{Ca} \qquad \text{eq. 23}$$

where *h* (m) is the cross-sectional dimension of the channel.

Above a certain critical capillary number, droplet breakup occurs. It is important to note that this critical value is system dependent as different values have been reported by various groups using different geometries.[77, 98, 99]

In order to facilitate formation of droplets, it is important to consider the relative viscosity between the discrete and continuous phases, in particular selecting a more viscous continuous phase.

4.3 Droplet manipulation

Several actions can be performed on droplets generated in a microlfuidic device: fission, fusion, mixing and sorting. Mixing is an important tool required for carrying out and studying the kinetics of biological and chemical reactions. Before a reaction between two reagents can occur, intimate contact between the component molecules must be realized through mixing but, due to laminar flow conditions inside microfluidic channels, when two fluids come into contact with each other there is no turbulent mixing and reagents meet only because of diffusion. Diffusion can be an efficient transport mechanism at the nano- and low micro-scale, but turns out inefficient at the higher micro- and macro-scale. Even if the diffusion distance is

small, the time required to completely mix the two fluids could be still too long. The approximate diffusion coefficient for small molecules is typically 5×10^{-10} m^2/s and for proteins 5×10^{-11} m^2/s. [100] Consequently, for a small molecule it will take 0.1 s to diffuse 10 μm, 10 s for 100 μm, and more than 27 h to diffuse 1 cm. Thus the same properties that allow adjacent miscible fluids to flow in distinct streams become a problem when the fluids have to be mixed.

If efficient mixing is required, for example to carry out chemical reactions, different strategies must be employed to address the problem of slow diffusive mixing under laminar flow.[101, 102] They can all be broadly classified as being either passive or active. Passive mixers rely on geometric properties of the channel or fluidic streams to maximize the area over which diffusion can occur, whereas active mixers rely on time-dependent perturbations of the fluid flow to achieve mixing.[103]

Passive mixers have found the widest use in synthetic applications due to their simplicity and operational flexibility. When a droplet moves through a straight channel, an equal recirculating flow is generated in each half of the droplet that touches the channel wall.[104] Fluids within each half of the droplet are mixed, but the halves remain unmixed and separated from each other. To enhance internal mixing within droplets, channel geometry is used to create chaotic advection to fold and stretch the droplet contents (**Figure 12a**).

Chaotic advection in microfluidic systems can be achieved by introducing obstacles within channels or on channel surfaces, or by modifying channel geometries, for example with the use of bends and turns. In each case, the modification acts to enhance stretching, folding and breaking of the flow. As the droplet traverses through a winding channel, the halves of the droplet experience unequal recirculating flows. One half of the droplet is exposed to the inner arc of the

winding channel, a shorter channel section, and thus a smaller recirculating flow is generated compared to the other droplet half which is exposed to a longer channel section (**Figure 12b**). The irregular motion along the walls promotes chaos and crossing of fluid streams since the fluid vortexes of each half are asymmetrical. The droplets achieve an alternating asymmetric flow pattern through the serpentine microchannels. The sharp turns also help to reorient the droplet so that it becomes thoroughly mixed as it goes through a series of stretching, reorientation, and folding (**Figure 12c**).[105] An advantage of this design is that the degree of mixing is determined by the length of the channel.

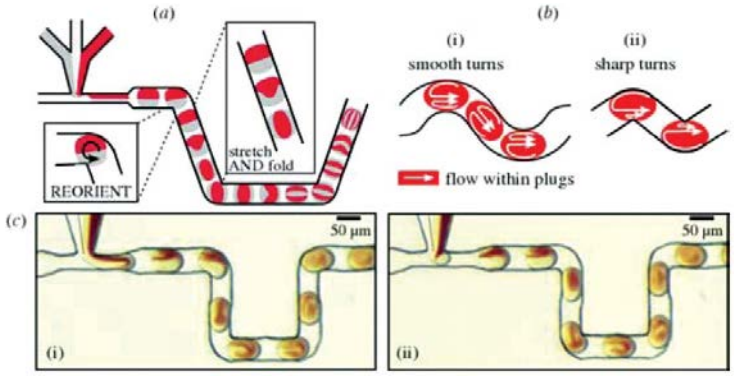

Figure 12. Passive mixing within droplets. (a–b) Schematic demonstrating mixing patterns within droplets inside winding channels. (c) Experimental results show the rotational pattern.

Active mixing is instead electrically controlled with either the droplets sandwiched between electrodes, or with the droplets lying on an array of electrodes. The droplets may also be separated by a hydrophobic dielectric layer and not in direct contact with the electrodes. Electric control allows droplets to be moved and mixed in a confined space whereas channel-based mixing requires more elaborate and long winding channels. Each droplet is also individually controlled and its mixing is not dependent on channel design or fluid flow rates.[106]

To perform a multiple-step reaction, reaction mixtures must be combined and split in a controlled manner. By using droplet-based microfluidics, reactions can be

combined by merging two droplets and also split by splitting one droplet into two smaller droplets.[107] Various methods have been developed for merging and splitting droplets. In passive fusion the device itself drives droplets at a precise position where fusion can occur. It can be controlled by varying flow rates and channel geometry or altering surface hydrophilicity selectively.[108] For example, in order to combine two parallel reactions, two sets of droplets can be formed in two parallel microchannels that converge into one main channel. The two sets of droplets will merge within the main channel if the frequency is matched between the two droplets.

Droplet fusion starts when two or more droplets are brought into contact. Increased pressure and surface tension will lead to drop coalescence.[109] The simplest way to promote passive fusion is to insert an expanded region along a channel.[110] The expanded region helps draining the continuous phase between the droplets and reduces droplets flow rates. Then drops enter again a narrower channel and this will promote fusion.

Again splitting is said to be passive if no external components or power sources are used. It is rather performed with the aid of the shear forces created by channel design at precise location in the microfluidic device. It can be controlled by varying the flow rate of the continuous phase and placing resistances along the channels. On the other hand active fission implies external power or electrical control of the splitting mechanism.

Sorting allows functions as the isolation of droplets of interest, purification of synthesized samples and the segregation of heterogeneous mix of droplets. It enables individual control of single droplets out of a population. Passive sorting relies on channel geometry modifications or gravity to distinguish the droplets to be sorted. As an example, a new size sorting mechanism that causes droplets to sort into two

different daughter channels under a fixed flow rate was demonstrated.[111] Droplet sorting by size was achieved in microfluidic channels through controlling the bifurcating junction geometry and the flow rates of the daughter channels. In size-based sorting using channel geometry, the microfluidic channels are designed so that the flow stream of the continuous phase carries the smaller satellite droplets into a side channel, whereas the larger primary droplets flow through the main channel.[112] Due to their smaller surface area, the satellite droplets are exposed to the flow projected from only the side branch whereas the larger droplets feel the higher velocity flow stream of the main channel.

An active sorting system employs an increased level of complexity, but provides more flexibility. Active sorting employs electrical control and has also been used as a mechanism to manipulate the droplets. A droplet-based microfluidic platform for the analyses of cells have been described that is able to dielectrophoretically sort drops sorted at high speed based on fluorescence.[113] This screening system operates as a drop-based FACS (Fluorescence-activated cell sorting) in that it interrogates individual cells and sorts them based on the results. However, unlike a traditional FACS, the cells remain encapsulated in drops and the entire reaction vessel is assayed and sorted. This methodology is not limited to reactions with cells or even to biological reactions. In this sense, drop-based microfluidics has many of the merits of both screening using microtiter plates and FACS.

5. GOLD NANOPARTICLES

Gold was the first metal to be transformed into a colloidal state. The "beautiful ruby fluid" formed upon the reduction of aqueous gold chloride with phosphorus dissolved in carbon disulfide was first described by Michael Faraday in 1857,[114] but it was not until 1908 that the color effects associated with colloidal gold nanoparticles (AuNPs) were rationalized by Gustav Mie.[115] The intense red color of AuNPs is due to the interaction of incident light with a collective oscillation of the free electrons in the particles, now known as localized surface plasmon resonance.

Today, AuNPs are synthesized using various methods and they have been the focus of extensive research activities.[116, 117] Surface and core properties of AuNPs can be engineered for a w ide range of bioanalytical applications[118] in which biomolecules and nanoparticles typically meet at the nanometer length scale.[119] Among different kinds of biomolecules, DNA is particularly suitable for applications in nanobiotechnology,[120, 121] and a number of different fields have benefited from such applications.

AuNPs are for several reasons the most widely used nanostructures for DNA detection,: simple synthetic procedures are required to obtain AuNPs with well-controlled diameters, shapes and optical properties; AuNPs are associated with high extinction coefficients ($2.7 \cdot 10^8$ $M^{-1}cm^{-1}$ at ~520 nm for 13 nm spherical AuNPs),[122] so slight aggregation may result in intense color changes; and the large surface area of nanoparticles allows hundreds of capture probes to be loaded, while the three-dimensional assembly of the probe lowers steric hindrance and favors target–probe hybridization.

Numerous synthetic strategies for the preparation of AuNPs have been reported.[123,124,125] The most widely adopted involves the chemical or electrochemical

reduction of Au(III) precursor compounds in the presence of a capping agent. The classic Turkevich–Frens method[126] uses citrate ions as the reducing/capping agent in order to electrostatically stabilize nanoparticles against aggregation.

AuNPs that can be prepared in a range of diameters (between 10 and 147 nm) with high degree of precision and accuracy, usually achieved through the careful selection of the experimental conditions, [127] like the ratio of the reducing/capping citrate agent to the Au(III) precursor derivative [the hydrogen/sodium tetrachloroaurate (III)][128]. The Turkevich–Frens method is used frequently even now, as the rather loose shell of citrates on the surface of the particle is easily replaced by other desired ligands with valuable functions. Once prepared, AuNPs are stable for long periods and, because they are generally employed at very low concentrations, they are cheap, even though the material from which they are made is proverbially expensive.[129]

Monodisperse AuNPs are red and exhibit a relatively narrow surface plasmon absorption band at 520 nm.[130] In contrast, aggregated AuNPs appear blue-purple in color, corresponding to a characteristic red-shift of the surface plasmon resonance. The aggregation is accompanied by a color change and it may be quantified spectrophotometrically.

AuNPs are unique because their nanoscale dimensions give rise to high reactivity and physical properties (electrical, optical, catalytic) that can be easily tailored by chemically modifying their surfaces. These fascinating size- and shape-dependent optical properties make AuNPs ideal nanomaterials for sensing applications. [131, 132]

High stability in electrolytic environments is required, which is not always easily achievable.[133] It depends on the balance between the repulsive and attractive

forces exerted between particles as they approach one another. Deryagin and Landau (1941) and Verwey and Overbeek (1948) developed a theory of the behaviour of colloidal systems that helps in understanding macromolecular labeling with gold particles. The so-called DLVO theory views the particles in a sol as consisting of two components producing opposite effects in aqueous suspension.[134] Van der Waals forces are the primary attractive force, whereas the overlap of electrical double layer of each particle causes a negative charge on the surface, leading to particle-particle repulsion and stabilizing the sol from aggregation. So as particles approach each other, an energy barrier must be traversed to overcome the repulsive character of the negative surface and enter the region of Van der Waals attraction (**Figure 13**).

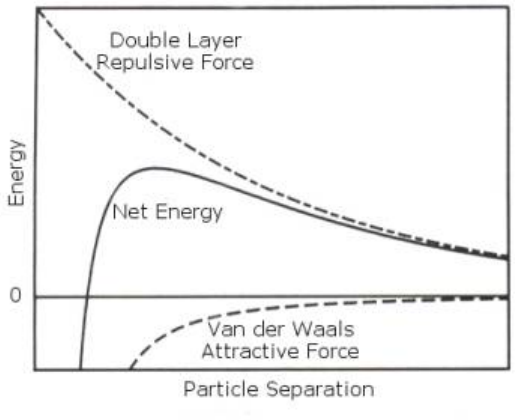

Figure 13. Variation of free energy with particle separation according to DLVO theory

This barrier can be breached by the addition of electrolytes to the solution that can mask the negative charge on each particle. At a certain electrolyte concentration the colloid will begin to collapse as the gold particles adsorb onto one another, forming large aggregates and ultimately falling out of suspension. Therefore if the particles have a sufficiently high repulsion, the dispersion will resist flocculation and the colloidal system will be stable. However if a repulsion mechanism does not exist then flocculation or coagulation will eventually take place. Therefore to maintain the

stability of the colloidal system, the repulsive forces must be dominant.[135] There are two fundamental mechanisms that affect dispersion stability:

- Steric repulsion, relying on the adsorption of polymers preventing the particle surfaces coming into close contact by steric repulsions.
- Electrostatic stabilization, based on the distribution of electrostatically charged species in the system.

Each mechanism has its benefits for particular systems. Steric stabilization is simple, requiring just the addition of a suitable polymer. However it can be difficult to subsequently flocculate the system if this is required, the polymer can be expensive and in some cases the used polymer is.

The generation of electrostatic repulsion between charged conjugates is the most common strategy to keep NPs separated in aqueous medium and, subsequently, stable under physiological conditions.[133, 136]

The theoretical implications of the DLVO theory in the case of gold conjugates have been extensively studied by Whitesides et al.,[137] who measured the stability of colloidal dispersions at different pH values and ionic strengths in the presence of a series of alkanethiols differing in the terminal functionality and showed an enhanced stability for the ionizable surfaces.

An increase in electrolyte concentration can be exploited to produce labelling, in place of aggregation. In fact, if macromolecules like proteins are present in the colloidal suspension, as the electrolyte concentration is raised to overcome the negative repulsion effects, then adsorption of protein on AuNPs will occur. The most common electrolyte additions in protein–gold labeling are NaCl or buffer salts. In practice, the addition of a protein to a suspension of gold nanoparticles will result in spontaneous adsorption on the surface of the gold particles due to electrostatic,

hydrophobic, and Van der Waals interactions.It is generally believed that the maximum adsorption occurs at or near the protein pI.[138, 139] This is the pH of net electrical neutrality for a protein, wherein any electrically induced repulsive or attractive forces are balanced.

The ultimate goal of AuNP surface modification with biomolecular systems is to preserve the properties of both the AuNP and the bound molecule. In fact, the surface-bound biomolecule must be stable and must retain its biorecognition properties, and AuNPs must retain their unique properties, such as strong surface plasmon absorption bands and light scattering.

After the milestone work from Mirkin's group,[140] who described the first colorimetric DNA sensor that utilized functionalized AuNPs in 1996, DNA-functionalized AuNPs have become popular sensing materials for DNA detection.

The functionalization of AuNPs with biomolecular systems has only been carried out with a limited number of strategies (**Figure 14**)[141]: ligand-like binding to the surface of the AuNP, (in these cases biomolecules are simply adsorbed either directly onto the AuNP surface or onto the shell of stabilizing ions or molecules around the nanoparticles); electrostatic adsorption of positively charged molecules onto negatively charged AuNPs through electrostatic interactions between biological molecules and (oppositely charged) nanoparticles; covalent binding between the biological molecule and the stabilizing shell around the AuNP; and affinity-based binding.

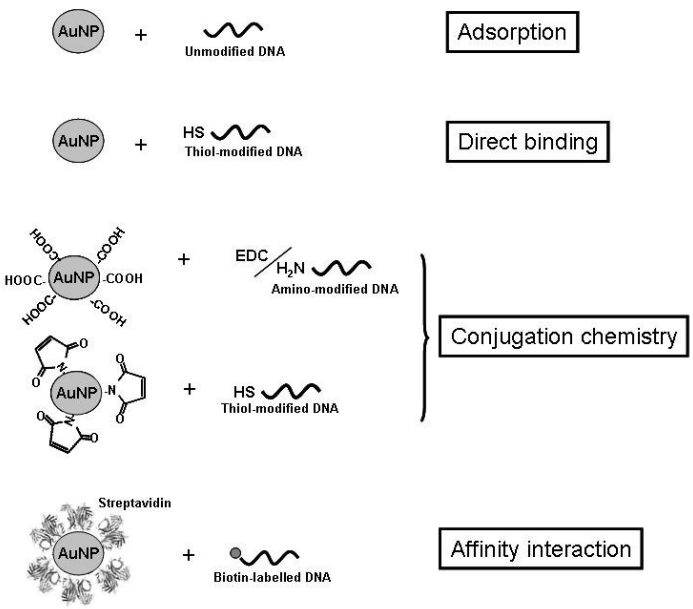

Figure 14. Schematic illustration of the strategies used in AuNPs functionalization

The binding of thiol groups to Au surfaces is widely used to immobilize up to several hundred thiol-modified oligonucleotides (ODNs) on a single AuNP. Oligonucleotide density on the AuNP's surface can be influenced by adjusting the excess ratio or by diluting with other ligands, such as short oligomers.[142] The method leads to the stable immobilization of ODNs on the AuNP surface and is more expensive than other immobilization procedures. Unfortunately, even under optimized conditions,[143] the binding of thiol-modified ODNs to gold nanoparticles does not occur quantitatively. Moreover, there is no easy direct synthesis of nanoparticles with exact ODN molecule-to-particle ratios.

On the other hand, the modification of AuNPs through electrostatic interactions between oligonucleotide bases and the surface of the AuNP is relatively simple and cheap. However, the binding achieved is not as stable as the covalent binding, particularly under high ionic strength conditions. The conformation of ODNS electrostatically adsorbed onto the AuNP surface represents another important issue to consider. An inconvenient conformation is expected to affect the hybridization

efficiency of nanoparticle-immobilized ODNs. Achieving a good balance between ODN surface coverage, particle stability, and hybridization efficiency is important in order to obtain functionalized AuNPs that can be used for sensing purposes. Appropriate surface coverage can be obtained by considering that proper salt conditions during the functionalization process induce a higher loading of DNA strands due to reduced electrostatic repulsion between the negatively charged oligonucleotide strands on the nanoparticle surface.[144] The use of oligonucleotide spacer segments helps to reduce electrostatic and steric interactions between surface-bound oligonucleotides and incoming complementary DNA stands involved in hybridization.

Conjugation chemistry can also be employed to covalently bind ODN to functional groups available on the nanoparticle surface. 1-ethyl-3-(3-dimethyl-aminopropyl)carbodiimide (EDC) chemistry is useful for binding amino-functionalized oligonucleotides to AuNPs with carboxylic groups,[145] while maleimide groups on the AuNP surfaces are used for thiol-modified oligonucleotides.[146]

Streptavidin-functionalized AuNPs have been used for the affinity binding of biotinylated oligonucleotides.[9, 147]

Metallic nanoparticles have been shown to greatly enhance DNA detection sensitivity when used for labelling purposes, as well as modifiers of transducers.[148,149]

The most widely used DNA detection approaches that rely on functionalized AuNPs are based on: methods that employ color changes in AuNPs upon nanoparticle aggregation (colorimetric detection—the best characterized example uses ODN-functionalized AuNPs capable of specifically hybridizing to the

complementary target for the detection of specific DNA sequences); methods that use AuNPs as a core/seed that can be tailored to include a wide variety of surface functionalities, thus yielding highly selective nanoprobes that can be used in combination with various signal transducers (QCM, SPR, etc.); electrochemical detection methods that benefit from the signal enhancement generated by metals deposited on the AuNP surface (silver enhancement); and methods that use AuNPs with alternative detection protocols (e.g., a lateral flow strip).

6. MATERIALS AND METHODS

6.1 SPRI experiments

6.1.1 Materials and reagents

Wild-type streptavidin (WT-SA) was purchased from Invitrogen (Italy). Nitrocellulose membrane filters were purchased from Whatman (UK). Trisodium citrate dihydrate, tetrachloroauric(III) acid, ethanol, dimethyl sulfoxide, hexane, sodium hydroxide solutions and 3,3′-Dithiodipropionic acid di(N-hydroxysuccinimide ester) (DTSP) were purchased from Sigma–Aldrich (Italy). Phosphate buffered saline (PBS) solutions at pH 7.4 (137 mM NaCl, 2.7 mM KCl, phosphate buffered 10 mM) were obtained from Amresco (Italy). Biotinylated oligonucleotide (DNAβ39) (**Figure 15**) was purchased from Thermo Fisher Scientific, Inc. PNA probes (**Figure 15**) (PNA-N: 5'-$(AEEEA)_2$-CTCTGGGTCCAA-3' and PNA-M: 5'-$(AEEEA)_2$-CTCTAGGTCCAA-3') were purchased from Panagene Inc.

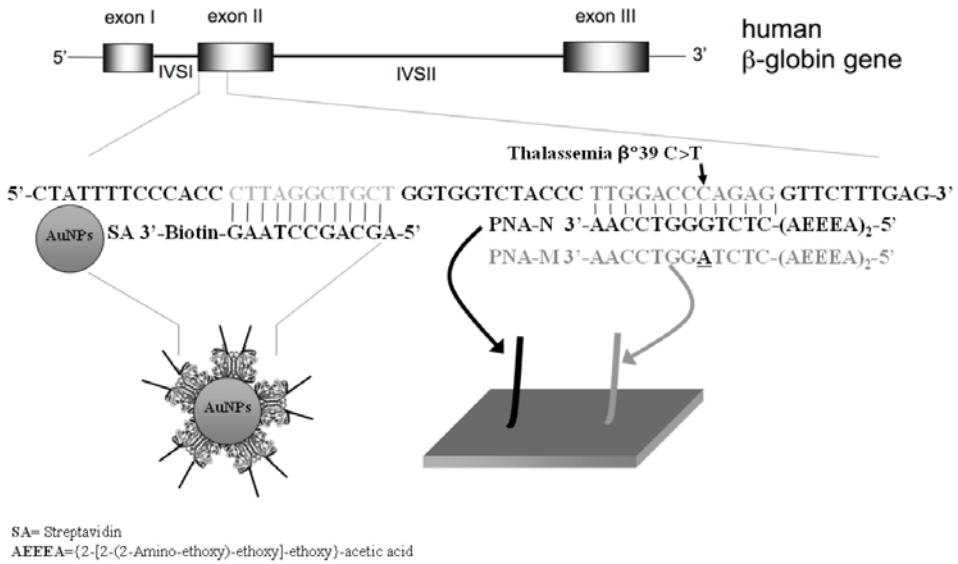

Figure 15. The location of the human β-globin gene is shown with the sequence targeted by the complementary PNA-N and PNA-M probes. PNA-N is complementary to the normal β-globin sequence while the PNA-M is complementary to the β39 mutated sequence. The position of the β39 C>T point mutation is also shown. The sequence of the DNAβ39 11-mer biotinylated oligonucleotide immobilized on the gold nanoparticles is also shown with the complementary targeted sequence.

SPRI gold chips were purchased from GWC Technologies (USA). Gold substrates were obtained by thermally evaporating a gold layer (450 Å) on to SF-10 glass slides. Chromium (50 Å) was used as the adhesion layer (**Figura 16**).

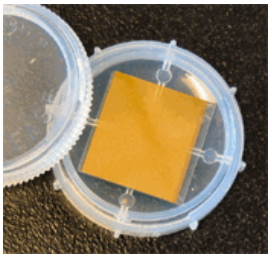

Figure 16. SPRi sensor.

6.1.2 SPRI experiments and data analysis

All the SPRI experiments were carried out by using an SPR imager apparatus (GWC Technologies, USA). SPR images were analyzed by using the V++ software (version 4.0, Digital Optics Limited, New Zealand) and the software package Image J 1.32j (National Institutes of Health, USA). SPRI provides data as PIUs (pixel intensity units) in a 0–255 scale. The signal may be converted to real change in reflectivity Δ%R, that corresponds to an absolute physical unit of measurement. In order to convert the results to Δ%R, the polarizer adjuster is rotated 90° left or right to change the polarization of light from "p" to "s". Since there is no SPR response to s-polarized light, all of the light will now be reflected off the gold surface and the CCD image for these regions will be white. If 100% of the s-polarized light reached the CCD camera, it would saturate the detector and the signal would not be accurately measured. For this reason, a neutral density filter is placed in front of the polarizer to reduce the light energy reaching the prism. Now an image can be acquired. V++ generates a text window containing reflectivity data for each ROI on the s-polarized image. These value are used for the adjustment of data to Δ%R using the following formula:

$$\Delta\%R = 100 \cdot I_p \cdot 0.85 \cdot (1\text{-}d) / I_s \qquad \text{eq. 24}$$

where d is the density of the filter used (a filter was employed that transmits only 10% of the light, d = 0,9) and I_p and I_s refer to the reflected light intensity detected using p- and s-polarized light, respectively.

The experiments were carried out by sequentially acquiring 15 frames averaged SPR images with 5 s time delay between them. Kinetic data were obtained by plotting the difference in percent reflectivity (Δ%R) from selected regions of interest (ROIs) of the SPR images as a function of time. The selected ROIs were chosen in

order to include all the SPR chip area involved by the surface interaction experiment. All the SPRI experiments were carried out at room temperature.

6.1.3 Microfluidic devices fabrication

A microfluidic device with six parallel microchannels (80 µm depth, 1.4 cm length, 400 µm width) and circular reservoirs (diameter = 400µm) at the ends of each channel was used for the study. It allowed an independent control of the interactions occurring on six different regions of the SPRI gold chip surface. The device was fabricated in poly(dimethylsiloxane) (PDMS) polymer through the well established replica molding technique.[150] Briefly, PDMS channels were created by replication from masters in polyvinyl chloride (PVC). Replicas were formed from a 1:10 mixture of PDMS curing agent and prepolymer (Sylgard 184, Dow Corning, USA). The mixture was degassed under vacuum and then poured onto the master in order to create a layer with a thickness of about 3-4 mm. The PDMS was then cured for at least 2 hours at 60 °C before it was removed from the masters. The PDMS mold bearing the negative pattern of the masters was peeled off and washed repeatedly with ethanol, hexane, ultra-pure water and dried before use. PEEK tubes (UpChurch Scientific) were inserted in the circular reservoirs in order to connect the PDMS microfluidic cell to an Ismatec IPC (Ismatec SA, Switzerland) peristaltic pump. The microfluidic device was assembled by fixing the PDMS mold on the SPRI gold chip surface, allowing independent functionalization and detection at six area on SPRI gold chip. (**Figure 17**). A refractive index (1.7200±0.0005) matching liquid (Cargille Laboratories, Inc.) was used to obtain the optical contact between the gold chip and the prism.

Figure 17. Representative SPRI image. The contrast was generated by the PBS running buffer continuous flow through six parallel microchannels

6.1.4 Estimation of Adsorbate Film Thickness from Measured SPR Response

Over a narrow range, the response to changes in bulk index of refraction η, in the absence of adsorption from the solution, can be approximated as linear: [151, 49]

$$\Delta\%R = m\Delta\eta = m(\eta_{final} - \eta_{initial}) \qquad \text{eq. 25}$$

For a metal surface coated by an adsorbate of thickness d and refractive index η_a, in contact with a solution of refractive index η_s, the SPR response in an adsorption process corresponds to either the shift in wavelength ($\Delta\lambda$) or angle of the SPR minimum ($\Delta\theta$) in reflected light intensity associated with changes in the index of refraction of the medium in contact with the metal surface of the SPR device, $\Delta\eta$, starting from the clean metal in contact with the same bulk solution (refractive index η_s).

The effective index of refraction for the bilayer, η_{eff}, is the properly weighted average of η_a plus η_s, Then it is possible to estimate the response to adsorption using eq.26 :

$$\Delta\%R = m(\eta_{eff} - \eta_s) \qquad \text{eq.26}$$

Since light is being used to probe this index of refraction, it is possible to assume that the proper weighting factor at each point in the bilayer structure should be proportional to the intensity of light at that point.

The evanescent electromagnetic field decays away exponentially into this medium with a characteristic decay length, l_d, of ~25-50% of the wavelength of the light.

Thus, the proper weighting factor in calculating this average refractive index should just be $[\exp(-z/l_d)]^2 = [\exp(-2z/l_d)$, Where z is the height above the metal surface (**Figure 18**).

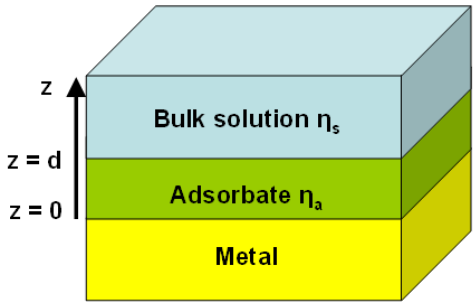

Figure 28. Schematic diagram of a thin metal film coated by an adsorbate of thickness d and refractive index η_a, in contact with a medium to be probed (a solution of refractive index η_s).

Thus, the effective index of refraction is calculated by averaging the refractive index over the depth of the whole structure. This average is therefore calculated with the depth integral:

$$\eta_{eff} = (2/l_d)\int_0^\infty \eta(z)\exp(-2z/l_d)dz \qquad \text{eq. 27}$$

where $\eta(z)$ is the refractive index at height z.

In the simple case where $\eta(z) = \eta a$ for $0<z<d$ and $\eta(z) = \eta s$ for $d<z<\infty$, the integral of eq. 27 reduces to

$$\eta_{eff} = \eta_a[1-\exp(-2d/l_d)] + \eta_s\exp(-2d/l_d) = \eta_s + (\eta_a - \eta_s)[1-\exp(-2d/l_d)] \quad \text{eq. 28}$$

Thus, the sensor response is:

$$\Delta\%R = m(\eta_{eff} - \eta_s) = m(\eta_a - \eta_s)[1-\exp(-2d/l_d)] \quad \text{eq. 29}$$

This equation, rearranged to solve for the adlayer thickness, can be used to estimate an adlayer thickness from a measured SPR response as well as to predict the response from a certain adlayer structure:

$$d = -(l_d/2)\ln(1-\Delta\%R/\Delta\%R_{max}) \quad \text{eq. 30}$$

where $\Delta\%R_{max}$ is the maximum response that would be measured for an infinitely thick adlayer, or:

$$\Delta\%R_{max} = m(\eta_a - \eta_s) \quad \text{eq. 31}$$

The constant m should be determined first from calibration curves, measuring the changes in intensity ($\Delta\%R$) due to changes in bulk refractive index ($\eta\Delta$) using bulk solutions with known refractive index.

In the special case where d is very small compared to l_d, eq. 30 reduces to

$$d = (l_d/2)(\Delta\%R/\Delta\%R_{max}) = (l_d/2)\Delta\%R/[m(\eta_a - \eta_s)] \quad \text{eq. 32}$$

so that the response is directly proportional to the thickness of the adlayer.

The average thickness (d) of a uniformly spread adlayer can be converted to surface concentration (θ) in molecules per cm^2. The conversion factor N is just the bulk number density of the adsorbate, in units of molecules per cm^3:

$$\theta \text{ (in molecules/cm}^2\text{)} = d \text{ (in cm)} \cdot N \text{ (in molecules/cm}^3\text{)} \qquad \text{eq. 33}$$

The bulk number density of the adsorbate (N) can be estimated from the bulk density of the adsorbate (ρ), in units of g/cm^3, just by dividing by the molar mass (MM) and multiplying by Avogadro's number (N_a). The proper value of ρ to use is the value for pure, condensed bulk adsorbate.

$$N \text{ (in molecules/cm}^3\text{)} = \rho \text{ (in g/cm}^3\text{)} \cdot N_a \text{ (in molecules/mol)} / MM \text{ (in g/mol)} \qquad \text{eq. 34}$$

6.1.5 PNA probe surface immobilization for SPRI experiments

The specificity of the detection of the β°39 thalassemia point mutation was demonstrated by using two PNA probes (**Figure 15**) complementary to the normal sequence (PNA-N) and the sequence carrying the β°39 mutation (PNA-M), respectively. The probes were immobilized on the DTSP-modified gold chips through the amine-coupling reaction between the N-hydroxysuccinimidyl ester ends of DTSP and the N-terminal group present on the {2-[2-(2-amino-ethoxy)-ethoxy]-ethoxy}-acetic acid (AEEEA) linker. The probes immobilization was obtained using 0.1 μM solutions in PBS (flow rate 5μL/min) that produced a mean surface coverage of $3 \cdot 10^{12}$ molecules cm^{-2}.

6.1.6 Genomic DNA hybridization experiments

The SPRI genomic DNA hybridization experiments were performed at room temperature by using 300 μL of 5 pg/μL (~ 2.6 aM) genomic DNA solutions which were adsorbed (flow rate 10 μL/min) on the PNA-N and PNA-M functionalized surfaces. The solutions were obtained by diluting with PBS 100 pg /μL solutions which were prepared no more than 48 hours before the experiment from the genomic DNA stock solutions (typical concentration ranging between 100 ng/μL and 200 ng/μL).

Before SPRI analyses, genomic DNA samples were fragmented by sonication (3 min, ELMA Transsonic T480/H-2) and vortexing (1 min, IKA Vortex GENIUS 3) and denatured at 95°C for 5 min. Strands re-association was prevented by 1 min cooling on ice of the samples before their introduction into the SPRI microfluidic apparatus. The DNA solutions were used no more than 1 minute after the previous treatment.

6.1.7 Synthesis and functionalization of gold nanoparticles

Gold nanoparticles (AuNPs) were synthesized by citrate reduction of $HAuCl_4 \cdot 3H_2O$ according to methods elsewhere described[152] and were characterized by UV–vis spectroscopy (NanodropTM 1000 and Agilent 8453 spectrophotometers) and transmission electron microscopy (TEM, Jeol JEM-2000 FX II, operating at 200 kV) (**Figure 19**).

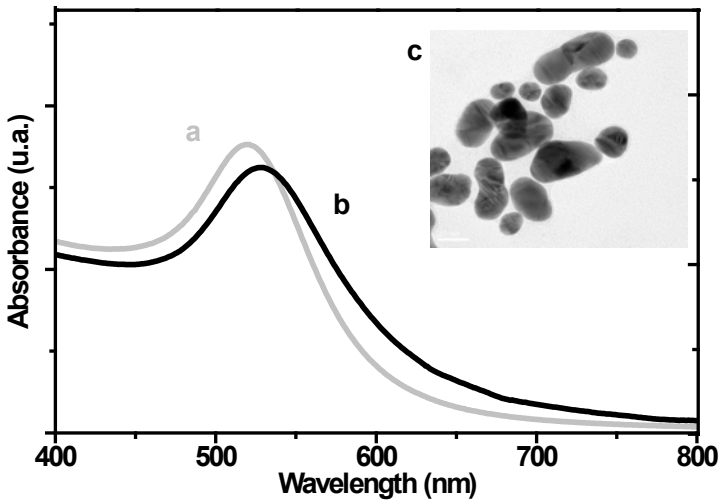

Figure 19. Representative UV-vis spectra of the citrate-stabilized AuNPs before (λ_{max} = 520 ± 1 nm) (**a**) and after (λ_{max} = 528 ± 1 nm) (**b**) the functionalization with the biotinylated DNAβ39 11-mer oligonucleotide sequence. (**c**) TEM image of the AuNPs (mean diameter = 20 ± 5 nm).

Briefly, 20 mL of trisodium citrate (38.8 mM) were quickly added with vigorous stirring to 200 mL of a boiling solution of $HAuCl_4$ $3H_2O$ (1mM). The colour of the solution changed from pale yellow to deep red in a few seconds. A complete reduction of trisodium citrate was obtained after 6-8 minutes under boiling. The solution was cooled to room temperature and filtered through a 0.45 μm mixed cellulose ester membrane filter. The AuNPs solution was stored at 4 °C in a clean brown glass bottle. Similar conditions assured nanoparticles stability for several months. The mean diameter of AuNPs was 20 ± 5 nm.

AuNPs were conjugated to the 3' end of biotinylated DNAβ39 (11-mer sequence, 5'-AGCAGCCTAAG-3', T_m = 34.0 C) as follows: 500 μL of a solution obtained by diluting (1:1) AuNPs with H_2O was added to 10 μL of a 1 mg/mL streptavidin solution after adjusting the pH to 8.5 (NaOH 0.1 M). The addition of the protein to a solution of AuNPs results in spontaneous adsorption on the surface of the gold nanoparticles due to electrostatic, hydrophobic and Van der Waals interactions.

The labeling process depends on several interactions: (a) the electrostatic attraction between the negatively charged gold particles and the abundant positively charged sites on the protein molecule, (b) adsorption phenomena involving hydrophobic pockets on the protein binding to the metal surface, and (c) the potential for covalent binding of gold to free sulfhydryl groups, if present (dative binding,).

AuNPs suspension containing streptavidin was incubated on ice for 1 hour and centrifuged (12500 rpm, 30 min, 23 °C). After the separation of the liquid phase, the modified AuNPs were suspended with 90 μL of water. 10 μL of DNAβ39 (100 μM in H_2O) were added to the streptavidin-conjugated AuNPs suspension and incubated for 30 min. After the centrifugation and the removal of the supernatant solution, DNAβ39-conjugated AuNPs were suspended in PBS buffer.

The actual concentration of the conjugated AuNPs stock solutions was obtained from UV–vis spectroscopy (ε_{528} =$2\times10^8 M^{-1}$ cm^{-1}) (**Figure 19b**).[153] Conjugated AuNPs stock solutions suitable for the SPRI ultrasensitive detection generated a λ_{max}=528±1 nm and were between 10 nM and 30 nM in concentration. Conjugated AuNPs for the SPRI signal enhancement were obtained from dilution of the conjugated AuNPs stock solution. The selection of an appropriate conjugated AuNPs final concentration is critical for the success of the experiments. The described experiments were conducted by using 0.1 nM conjugated AuNPs solutions (in PBS).

6.2 Microfluidics experiments

6.2.1 Materials and reagents

3M™ Fluorinert™ Electronic Liquid FC-3283 was used as the carrier fluid in all droplet-based microfluidics experiments. 1*H*,1*H*,2*H*,2*H*-perfluoro-1-octanol

(PFO) 97%, fluorescein, tris-(hydroxymethyl)-aminomethane (TRIS), dNTPs, Dimethyl sulfoxide (DMSO), DL-Dithiothreitol (DTT) and $MgCl_2$ were purchased from Sigma-Aldrich. The Olea europaea L. (Cultivar ogliarola) genes were chosen to demonstrate the rapid, simple and selective detection in the droplet microfluidic platform using a PNA-Molecular Beacon (PNA-MB) with the structure reported in **Figure 20**.

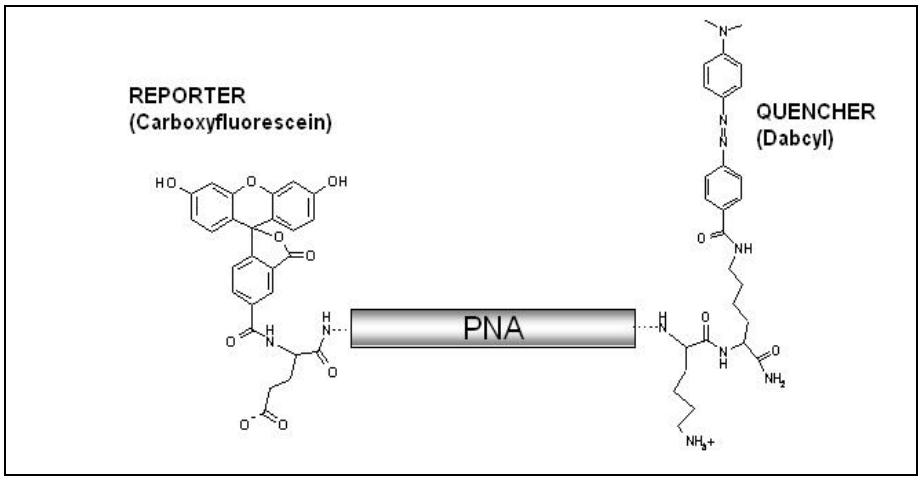

Figure 20. PNA-MB general structure.

There are no complementary sequences at either ends of the molecular beacon and thus there is no stem portion. Indeed it has been seen that interaction between reporter and quencher, perhaps mainly hydrophobic, is sufficient to keep the beacon in a closed state in solution when the target sequence is not present.[154] Carboxyfluorescein was the reporter and Dabcyl the quencher in the molecular beacons used in this work. Fluorescein has an absorption maximum at 494 nm and an emission maximum at 521 nm (in water). Dabcyl (4-[4-(Dimethylamino)phenylazo]benzoic acid) is a non fluorescent chromofore (a dark quencher) whose absorption maximum is at 474 nm. There is not a perfect overlap between the spectral properties of the two moieties, in terms of good

reporter/quencher pair, but dabcyl can still quench fluorescein emission to a sufficient extent.

It should be noticed that these two moieties are covalently attached to the PNA sequence via a linker that contains a positively charged amino acid (arginine) on one side and a negatively charged amino acid (glutamate) on the other. Salt bridge formation between these two amino acids helps keeping the stemless molecular beacon in a closed state.

Sequences and the acronyms of oligonucleotides (Thermo Scientific, Italy) for droplet-based microfluidic experiments are listed in **Table 1**.

Acronym	Description	Sequence
OGL	*Cultivar ogliarola* target sequence	5'-GGT GAA TGA GTA A-3'
mOGLA	*Cultivar ogliarola* inner mismatched sequence (T→A)	5'-GGT GAA **A**GA GTA A-3'
mOGLG	*Cultivar ogliarola* Inner Mis-Match Sequence (T→G)	5'-GGT GAA **G**GA GTA A-3'
mOGLC	*Cultivar ogliarola* Inner Mis-Match Sequence (T→C)	5'-GGT GAA **C**GA GTA A-3'
mOGLT	*Cultivar ogliarola* Outer Mis-Match Sequence (A→T)	5'-GGT GAA TGA GT**T** A-3'
Ctr	Unrelated control sequence	5'-AAG CTG ACT CTA G-3'
OPF	Opener oligonucleotide forward	5'-TGC AGA GC G GGA AAT TGT GA-3'
OPR	Opener oligonucleotide reverse	5'-CTC TGT GAG GAT TTT C AT CA-3'
PNA-MB	PNA molecular beacon complementary to a tract of *Cultivar Ogliarola* actin gene	Fluo-Glu-TTA CTC ATT CAC C-LysLys-(dabc)-NH_2[a]
Primer Fw	Forward Primer for PCR amplification	5'-GGC TGG TCG TGA CCT TAC TG-3'
Primer Rev	Reverse Primer for PCR amplification	5'-GAA GTC TCA AGC TCC TGC TCA-3'

Table 1: Acronyms and description of target and probe sequences

Differently concentrated oligonucleotide solutions were obtained by dilution with 10 mM TRIS buffer. Ultra-pure nuclease free water (Milli-Q Element, Millipore) was used for all the experiments.

The hairpin fluorescence probe, the short primer, the target related to the Roundup Ready soybean genome and random DNA oligonucleotides for the sensitive DNA amplified detection method, based on isothermal strand displacement polymerization (CSDP) reaction, were from Thermo Fisher Scientific. Klenow Fragment (3′→ 5′ exo-) was from MedClone s.r.l.

Two Harvard 33 Twin syringe pumps (Harvard Apparatus) were employed to handle Hamilton syringes. Pharmed BPT tubing (ID=0.25 mm, Cole Parmer) were used to connect syringes to microfluidic device inlets. A Leica DMI4000 B inverted microscope equipped with a Leica DFC360 FX monochrome digital camera was used to observe droplet generation and to perform fluorescence analyses. PNA-MB fluorescence was stimulated with filtered radiation produced with a Leica EL600 mercury short-arc reflector lamp. ImageJ 1.42 software was used for fluorescence data analysis.

In order to minimize the influence of both instrumental instability and background fluorescence, the fluorescence generated by PNA-MB in the presence of the complementary target sequence was subtracted from the intrinsic fluorescence of PNA-MB in a buffer solution alone. Control experiments were carried out by detecting fluorescence generated by PNA-MBs in the presence of unrelated DNA sequences. Data shown were obtained by averaging signals generated by five different droplets.

6.2.2 PCR amplification

DNA extraction from leaves of two different *Olea europaea L.* cultivars (Cultivar ogliarola and Cultivar ascolana) was carried out using the CTAB method described by Doyle and Doyle, with minor modifications.[155] PCR amplifications were carried out in a PCRsprint Thermal Cycler (Thermo Hybaid, Basingstoke, UK) using Blue Taq (Euroclone) , the primers reported in **Table 1** (Sigma Genosys), and the following conditions: 1 cycle of DNA denaturation and Blue Taq activation at 95 °C for 5 min; 40 cycles consisting of DNA denaturation at 95 °C for 50 s, primer annealing at 60 °C for 50 s and elongation at 72 °C for 50 s ; one step of final elongation at 72 °C for 5 min. Products length is 150 bp. PCR mixture used in the experiments consist of PCR buffer (50 mM KCl, 2 mM NaCl, 10.4 mM TRIS-HCl, pH 8.3, 2 µM EDTA, 20 µM DTT, glycerol 1%, Tween-20 0.014%), 3 mM $MgCl_2$, 0.2 mM dNTP, 0.2 µM primer Rev, 0.2 µM Primer FW, 0.1 units/µl Taq polymerase, 13 ng/µl dsDNA for Cultivar Ogliarola sample (0.13 µM in dsDNA) or 15 ng/µl dsDNA for Cultivar Ascolana sample (0.15 µM in dsDNA). The content of DNA after PCR was measured using Qubit fluorometer (Invitrogen) with reagents for dsDNA.

6.2.3 Amplicons pre-treartment for microfluidics experiments

PCR amplicons were treated before their injection into the droplet microfluidic device in order to allow the target sequence to be locally exposed to the PNA-MB complementary probe. For this reason 10 µL of a mixture of PCR amplicon (0.1 µM) and both OPF and OPR openers (each 30 µM) was heated at 95ºC for 5 minutes

in order to achieve dsDNA denaturation. OPF and OPR openers (**Table 1)** were each complementary to one of two sequences positioned laterally and not overlapping to the sequence targeted by the PNA-MB probe. The interaction between openers and denatured amplicons prevented the re-association of the amplicon strands[156] thus facilitating the PNA-MB probe interaction with target sequence. The openers hybridization with the complementary sequences was favoured by maintaining the denatured mixture at 55ºC for 1 minute.

The experiments were performed by introducing with a calibrated syringe (Hamilton) 1 µl of the treated PCR products into the tubing connecting the pump to the droplet microfluidic device.

6.2.4 Circular Strand Displacement Polymerization (CSDP) Reaction

The sensitive DNA detection method based on isothermal strand displacement polymerization reaction relies on the use of a hairpin fluorescence probe, a primer and a polymerase.[157] The hairpin fluorescence probe possesses a stem-loop structure with a fluorophore and a quencher moieties linked to the ends of the stem. The stem is 11-nt sequences long, and the loop is complementary to the target. The primer is 8-nt sequences long, which is complementary to the stem region of the probe at 3'-end. In the absence of the target, the probe is unable to anneal with the primer to induce a polymerization reaction. However, in the presence of target DNA, the probe hybridizes with it and undergoes a conformational change, leading to stem separation. Following this process, the primer anneals with the open stem and triggers a polymerization reaction in the presence of dNTPs/polymerase. Next, in the process of primer extension, the target is displaced by the polymerase with strand-displacement activity, after which a complementary DNA is synthesized, forming a

probe–cDNA complex (**Figure 21**). Finally, the displaced target recognizes and hybridizes with another probe, triggering the next round of polymerization reaction.

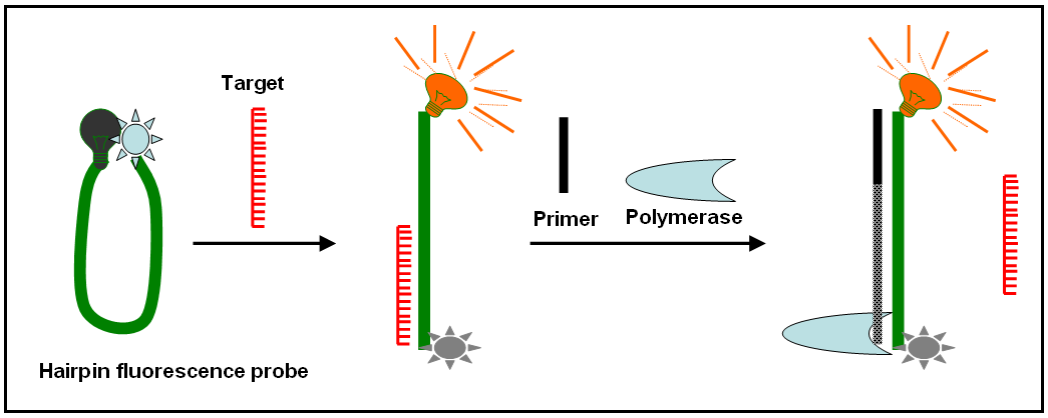

Figure 21. The mechanism of circular strand-displacement polymerization reaction for isothermal amplified detection of DNA.

The described method allows hybridization, polymerization reaction and displacement to occur cycle-after cycle, producing, at the same time, an amplified fluorescent signal sufficient to indicate the presence of trace amount of target DNA. In order to achieve a good amplification, it is important to accurately design the hairpin fluorescence probe. The stem of the probe should be long enough to ensure that stem hybridization affinity will be stronger than hybridization affinity with the primer. Therefore, in the absence of target, the primer does not induce polymerization reaction. On the other hand, a stem that is too long would restrain hairpin probe conformational change upon hybridization with target. Hence, in this work, the stem consisted of 11-nt-long sequences, thus forming a structure stable enough to prevent the primer from annealing with duplex stem (**Figures 22 and 23**)

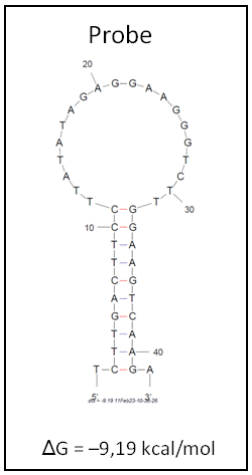

Figure 22. Structure of the hairpin fluorescence probe (ΔG = –9,19 kcal/mol).

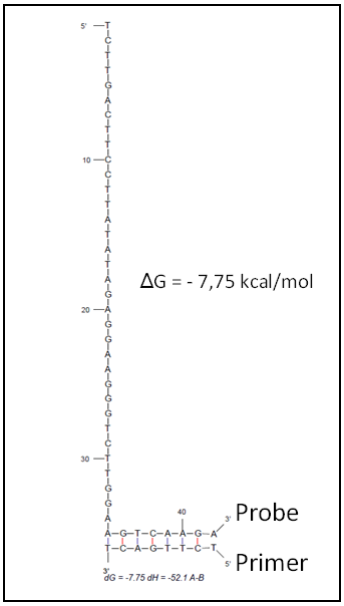

Figure 23. Structure of the hairpin fluorescence probe after hybridization with the primer (ΔG = -7,75 kcal/mol)

A fluorophore (6-FAM) and a quencher (Black Hole Quencher 1, BHQ-1) are linked to the ends of the stem of the hairpin fluorescence probe. BHQ-1 is classified as a dark quencher (a non-fluorescent chromophore) and is extensively used as the 3'-quencher moiety in a variety of FRET detection probes. It has an absorbance maximum at 534 nm and an effective absorbance range between 480-580 nm. The

use of a dark quencher in a FRET probe generates a quite low background fluorescence (and thus better signal-to-noise ratio).

In order to open long stem hairpin probe upon hybridization with target, a 'shared-stem' structure is designed, where one arm of the stem participates in either hairpin formation or target hybridization, i.e. besides the loop region, six bases of the stem at 5'-end is complementary to the target (**Table 2**).

5' AAGACCCTTCCTCTATATAAGGAAGT TTT 3'	**Full-Match Target Sequence**
5' TGGCTAGAGTAGAGTGAGCTAATCAA TTT 3'	**Random DNA**
5' 6-FAM TCTTGACTTCC TTATATAGAGGAAGGGTCTT GGAAGTCAAGA BHQ1 3'	**DNA beacon Sequence**
5' TCTTGACT 3'	**Primer Sequence**

Table 2. Sequences of the hairpin fluorescence probe and oligonucleotides

Two different samples were prepared to identify the hybridization feature of the hairpin fluorescence probe: sample A containing a random single-stranded DNA (control DNA); sample B containing full-match target DNA, with a sequence related to the genetically modified Roundup Ready soybean genome (**Figure 24**).

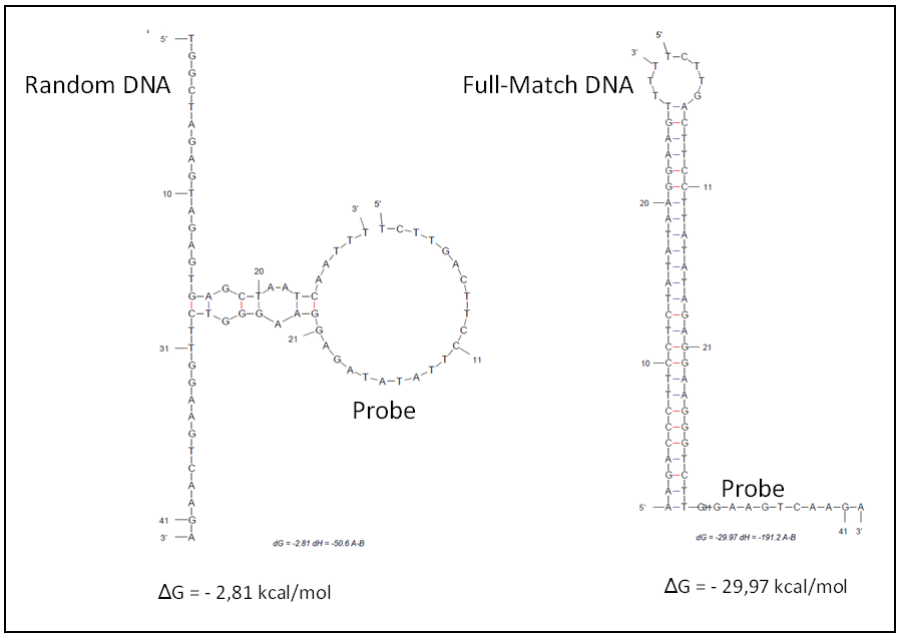

Figure 24. Hybridization of the probe with random and full-match DNA.

All measurements were performed in a microchannel by using less than 10 µl of a solution containing 0.12 µM probe, 0.12 µM primer, 10 U polymerase Klenow fragment exo-, 240 µM dNTPs, 6% DMSO, 1 mM DTT, 5mM $MgCl_2$ in 50mM Tris–HCl (pH 8.0). Samples were incubated at 37 °C out of the device for 20 minutes or 1 hour and then injected in the microchannel or first injected in the microchannel and there incubated at about 37 °C for 30 minutes.

6.2.5 Microfluidic devices fabrication

Microfluidic devices were fabricated in poly(dimethylsiloxane) (PDMS) polymer in agreement with established methods.[158] The irreversible adhesion of PDMS molds on microscope cover glasses was obtained after 30 seconds air plasma etching of cleaned surfaces using a Femto Diener Electronics plasma cleaner system with a 40 kHz generator. After the air plasma etching, treated surfaces were quickly placed in contact with each other and the new device placed at 60 ºC for 30 minutes. Microfluidic devices were used after at least 24 hours from their fabrication in order to allow the PDMS hydrophobic surface to be recovered after the plasma treatment. In fact, droplet microfluidic devices where water-in-oil droplets were produced required hydrophobic channel walls in order to facilitate their interaction with the carrier fluid. A schematic layout of the microfluidic device for the droplet-based DNA detection is shown in **Figure 25**.

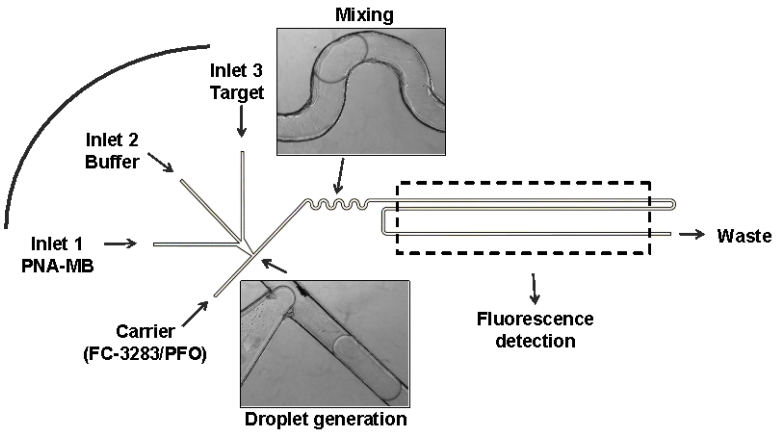

Figure 25. Scheme of the microfluidic device used for the droplet-based nucleic acid detection.

In order to obtain water-in-oil (W/O) emulsions, the continuous phase typically consists of oils or water-immiscible organic solvents, which tends to be more viscous than water. The surface of channels should be treated to ensure that the carrier fluid (and not the aqueous phase) preferentially wets the channel wall. In addition, the surface tension between the aqueous phase and the carrier fluid should be lower than the surface tension between the aqueous phase and the channel wall. Surfactants can be used within the carrier fluid to lower the surface tension between the aqueous phase and the carrier fluid. However, this surface tension should not be lowered too far as the capillary number Ca of the flow must be low to favor the formation of plugs.[159] Perfluorinated liquids are optimal carrier fluids for the formation of plugs, because they are considered to be chemically and biologically inert. Fluorinated surfactants can be used to control the surface chemistry at the interface between the aqueous phase and the fluorinated phase.[160] They are insoluble in the aqueous phase and arrange themselves at the interface between the aqueous and fluorous phases. Plugs are encapsulated in a thin layer of carrier fluid, so different surface properties can be obtained by simply changing the surfactant in the fluorinated carrier fluid without requiring functionalization of the microchannel wall.

PNA-MB probes and target sequences were introduced through Inlet 1 and Inlet 3, respectively. A continuous flowing of buffer solution was maintained through Inlet 2 in order to prevent mixing of probe and target solutions before droplets formation. The water-immiscible fluorinated carrier fluid (FC-3283/PFO 10:1) was continuously flowed through the main channel and droplets containing a mixture of nanoliter portions of solutions flowing through inlets 1, 2 and 3 were formed. The chaotic advection rapid mixing of multiple reagents isolated in droplets was obtained by moving droplets through winding channel.

6.3 Tube cleaning

Before each set of experiments, tubes were washing following a procedure proposed by David G. Myszka.[161] Solutions employed are reported in **Table 3**.

Solution	Time (min)
0,5 % SDS;	10
6 M Urea	10
1% Acetic acid	10
0,2 M Sodium bicarbonate	10
Water, 40 ºC;	20
Running buffer.	30

Table 3. Solution employed in washing procedure

7. RESULTS AND DISCUSSION

7.1 SPRI analysis of non amplified human DNA

Detected DNA samples, provided by group of Prof. Gambari at the Ferrara University, are genomic DNA samples extracted from individuals affected by β-thalassemia, an inherited autosomal recessive blood disease. Normal hemoglobin has four protein chains—two α-globins and two β-globins. β-thalassemia occurs when there is a defect in a gene that helps control of production of these proteins. The genetic defect results in reduced rate of synthesis of one of the globin chains that make up hemoglobin. Reduced synthesis of one of the globin chains can cause the formation of abnormal hemoglobin molecules, thus causing anemia, the characteristic presenting symptom of the thalassemias.

There are two main types of thalassemia:

- α-thalassemia occurs when a gene related to the alpha globin protein is missing or mutated: production of the α-globin chain is affected;
- β-thalassemia occurs when similar gene defects affect production of the β-globin protein.

β-globin chains are encoded by a single gene on chromosome 11, so β-thalassemias are due to mutations in the HBB gene on chromosome 11. Over 170 different mutations have been identified resulting in the β-thalassemias. In particular, in β°39 mutation, the sequence of codon 39 (CAG) is mutated to TAG.

Any given individual has two β-globin alleles. If only one β-globin allele bears a mutation, patients are heterozygous for β-thalassemia. Afflicted individuals harbor one normal β-globin gene and one that harbors a mutation leading to production of reduced or no β-globin. Thalassemia minor individuals are generally asymptomatic.

If both alleles have thalassemia mutations, β-thalassemia is referred to as thalassemia major. Patients are homozygous for the β-thalassemia mutation and require frequent blood transfusions for survival.

By using PNA probes, it is here demonstrated the ultrasensitive nanoparticle-enhanced SPRI detection of non-amplified genomic DNA sequences down to a 2.6 aM (2.6 10^{-18} M) concentration, maintaining a high selectivity in the recognition of single nucleotide mismatch. In particular, it is possible to discriminate between normal, β°39 homozygous and β°39 heterozygous non-amplified genomic DNAs. The experiments were carried out by using two 12-mer PNA sequences, PNA-N and PNA-M probes, specifically designed to identify the normal β-globin sequence and the β°39 mutated sequence respectively.

The strategy used for the ultrasensitive detection of SNPs in non-amplified genomic DNA is shown in **Figure 26**.

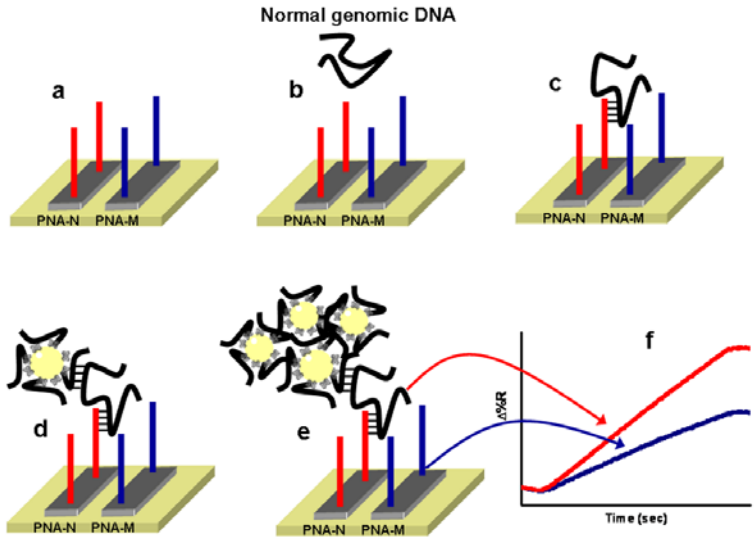

Figure 26. Pictorial description of the nanoparticle-enhanced SPRI strategy used to detect the normal, β°39 heterozygous and β°39 homozygous genomic DNAs. In order to simplify the pictorial representation only specifically adsorbed DNA is represented. Non-specifically adsorbed DNA is also present on the surface and contribute to generate the SPRI detected signal.

The genomic DNA was extracted from blood samples of healthy individuals and β-thalassemia patients and quantified by using a standard spectroscopic method. Working samples were obtained by dilution to a genomic DNA concentration of 5 pg/μL. This concentration was used because usually in prenatal diagnosis a small amount of amniotic fluid, which contains fetal tissues, is extracted from the amniotic sac surrounding a developing fetus, and the fetal DNA is examined for genetic abnormalities. Using such a low concentration, it would be possible to avoid this procedure, analyzing directly the DNA extracted from the blood of the mother. Normally genetic studies cannot be performed on maternal blood the concentration of fetal DNA is too low also for the amplification process. In fact, PCR cannot be performed on samples with a concentration lower than 1 ng/μL.

The spatially separated immobilization of the PNA-N and PNA-M probes was obtained by injecting PNA-N or PNA-M solutions (0.1 μM in PBS, flow rate 5 μL min^{-1}) (**Figure 27**) into parallel microchannels in contact with the DTSP-modified gold surface. The AEEEA spacer was used in order to minimize surface effects caused by the steric hindrance of the immobilized systems. A mean thickness of 1.6 nm was calculated for the deposited probe layer. A mean PNA-N and PNA-M surface coverage of about 3 x 10^{12} molecules cm^{-2} was obtained by multiplying the mean adlayer thickness value by the bulk number density of the adsorbate (molecules nm^{-3}). The latter parameter was estimated from Park et al.[162] Similar surface coverage values have been reported to minimize both steric interactions between adjacent probes as well as electrostatic interactions between target molecules.[163, 164]

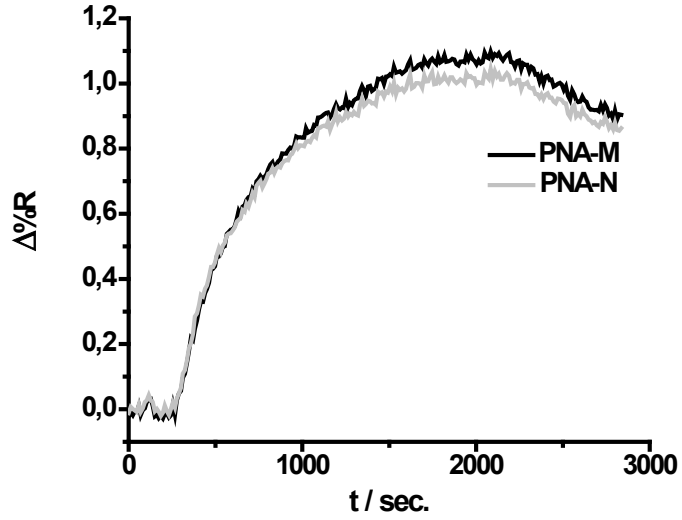

Figure 27. Representative changes in percent reflectivity (Δ%R) over time obtained for the immobilization of the PNA-N and PNA-M probes at 0.1 μM in PBS.

A typical experiment was performed by detecting the SPRI multiplex responses from three different DNA samples which were respectively normal, homozygous and heterozygous.

Both alleles of the β-globin gene are normal (βN/ βN) in genomic DNA of unaffected individuals while they are both affected by the β°39 point mutation in homozygous DNA (β°39/ β°39). Heterozygous DNA carries the β°39 point mutation only in one of the two alleles (β°39/ βN). Before the SPRI detection DNA samples were sonicated, denatured by heating to 95°C for 5 m in, rapidly cooled and incubated for 1 min on ice immediately before the SPRI analyses. 300 μL of each solution were then directly fluxed into each of six microchannels (flow rate 10 μL/min) in order to allows the direct adsorption of each of the three samples on the PNA-N and PNA-M functionalized surfaces.

The specific SPRI response patterns obtained when normal, homozygous or heterozygous DNAs were each allowed to interact with the two different PNA probes

provided a robust control of the experiment outcome. In fact, while normal DNA was expected to interact with only the PNA-N probe, different interactions were expected from homozygous and heterozygous DNAs: *i.e.*, interaction between homozygous DNA (β°39/ β°39) and only PNA-M probe and interactions between heterozygous DNA (β°39/ βN) and both PNA-N and PNA-M probes.

The direct absorption of the above mentioned 5 pg/μL solutions on the PNA-N and PNA-M functionalized surfaces failed to detect target DNA since generated SPRI signals close to the instrumental noise (**Figure 28**).

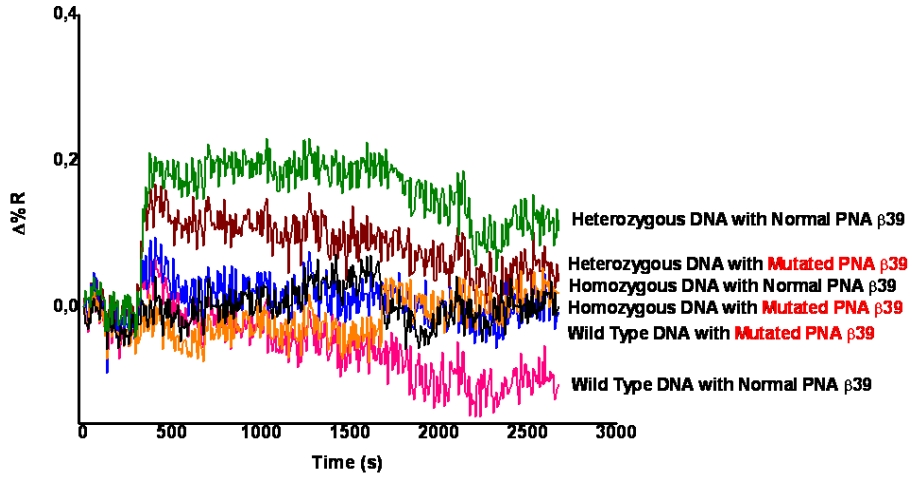

Figure 28. Representative change in percent reflectivity (Δ%R) over time obtained for the interaction between the surface immobilized PNA-N and PNA-M probes and the 5 pg/μL DNA samples (homozygous, wild-type and heterozygous).

Ultrasensitive detection of the genomic DNA targets hybridization was achieved by using AuNps conjugated to the DNAβ39 11-mer oligonucleotide complementary to a tract of the target DNAs not involved in the hybridization with the PNA probes (**Figure 15** and **26d**). By using this approach, a significant increase of the detected SPRI signals was obtained. **Figure 29** shows the SPRI change in percent reflectivity (Δ%R) over time (**Figure 29 a,b,c**) and a r epresentative SPR

difference image (**Figure 29 d**) obtained with 5 pg/μL solutions of non-amplified normal, heterozygous and homozygous genomic DNA.

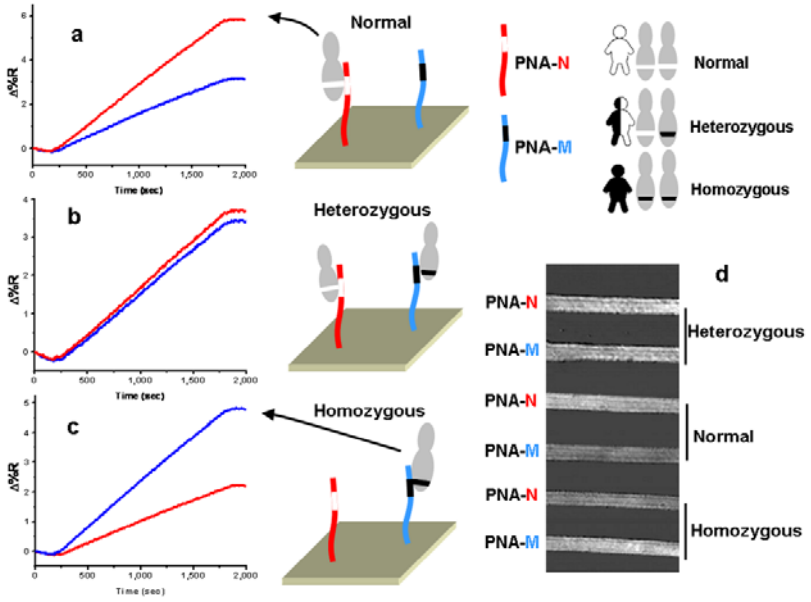

Figure 29. Time-dependent SPRI curves obtained after the adsorption of conjugated AuNps on normal (a), heterozygous (b) and homozygous (c) DNAs adsorbed to the surface immobilized PNA-N (red curve) and PNA-M (blue curve) probes. 5 pg/μL solutions of genomic DNAs were used for the experiments. A representative SPR difference image demonstrating the DNA parallel detection is also shown (d).

In normal individuals, where identical alleles of the non-mutated gene are present on both homologous chromosomes, DNA strands are complementary only to PNA-N on the surface of the sensor. Conversely, in homozygous individuals identical alleles of the mutated gene are present on both homologous chromosomes; DNA strands are complementary only to PNA-M on the surface of the sensor. As expected, normal (βN/βN) DNA preferentially hybridizes with the PNA-N probe while homozygous (β°39/β°39) DNA preferentially hybridizes with the PNA-M probe. In heterozygous individuals, two different alleles occupy the gene's position on the homologous chromosomes: one allele is normal while the other is mutated. Heterozygous sample hybridizes with both PNA-N and PNA-M probes with strikingly similar efficiency.

Replicated experiments were carried out by using genomic DNAs from 4 normal (βN/βN) individuals and 14 β-thalassemia patients (7 homozygous β°39/β°39 and 7 heterozygous β°39/ βN). (**Figure 30**) shows the ratio between the Δ%R caused by the nanoparticle-enhanced SPRI detection of the interaction between the DNA target and the PNA-N probe ($\Delta\%R_{PNA\text{-}N}$) and the Δ%R caused by the detection of the same DNA target and the PNA-M probe ($\Delta\%R_{PNA\text{-}M}$).

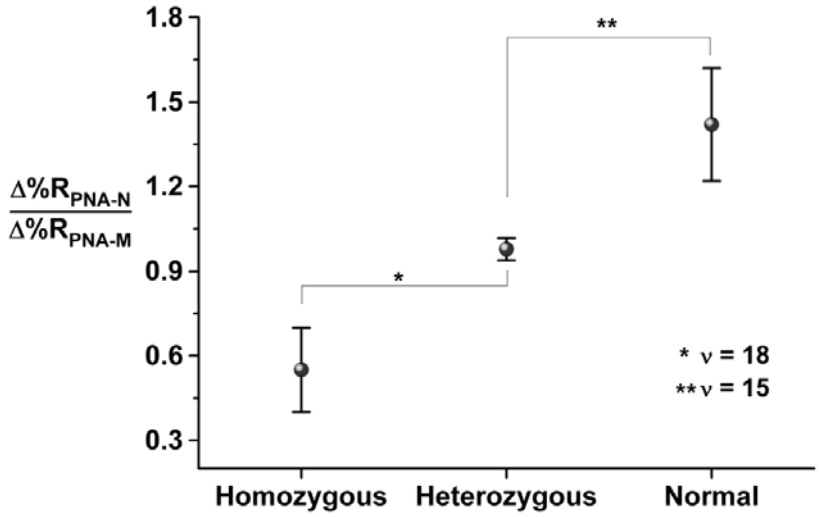

Figure 30. Mean $\Delta\%R_{PNA\text{-}N}/\Delta\%R_{PNA\text{-}M}$ ratio values obtained from replicated independent experiments. Error bars represent the 99% confidence interval (CI) of the mean. The asterisks (*, **) indicate statistically different values (t-test; p-value<0.0001). ν represents the degrees of freedom.

Data obtained clearly indicate that homozygous (β°39/β°39), heterozygous (β°39/βN) and normal (βN/βN) DNAs generated $\Delta\%R_{PNA\text{-}N}$ and $\Delta\%R_{PNA\text{-}M}$ responses whose ratios were different from one another (two-tailed t-test, level 99%, P< 0.0001).

Considering a molecular weight of about 1.9 10^{12} for the human genome (genome size about 2.9 Gb)[165,166] it is possible to conclude that the described method

can selectively discriminate between normal, β39 homozygous and β39 heterozygous DNA solutions down to a 2.6 aM concentration (5 pg/μL) by using only about 470 molecules of the genomic DNA.

The amplification of the signal arising from the use of AuNPs can be explained considering that due to their uncharged backbone, the PNA molecules form a neutral layer when immobilized on the gold surface. However, PNA is able to capture selectively a large ssDNA fragments, thus creating a negatively charged layer. This event occurs only if the target sequence is present in the genomic DNA used. Due to the protocol used, which minimizes re-annealing of DNA during analysis, the captured DNA remained in the form of single strand, while the flow in the microfluidic channel eliminated the excess DNA present and the strand complementary to the captured one, thus exposing the target sequence for the nanoparticle-linked oligonucleotide.

It is useful to highlight that, even after fragmentation, fragments still remain very large molecules since they are expected to comprise from hundreds to thousands of base-pairs. It is assumed that more than one nanoparticle is deposited on the surface for each DNA molecule captured. The deposition process, however, is favoured by a specific adsorption event, since the presence of a complementary oligonucleotide on the gold-nanoparticle is necessary to produce an increased positive signal.

The specific architecture of the SPRI interface forces the conjugated AuNPs to interact with large DNA fragments carrying both negatively charged groups and moieties (bases) able to establish weak interactions (van der Waals) with the conjugated AuNPs. The interface environment is supposed to alter the nanoparticle

stabilizing conditions at the interface, leading to AuNPs aggregation. The initial aggregation of AuNPs is proposed to constitute a sort of nucleation point around which other conjugated AuNPs aggregate.

The ultrasensitive detection process can therefore be described as follow. Adsorption of conjugated AuNPs, driven also by non-crosslinking interactions with the surface, is obtained when DNA fragments are retained both specifically and non-specifically by the PNA-modified surface. The initially adsorbed AuNPs activates an exponential accumulation of further AuNPs on the surface, which is favoured by the specific interaction between the oligonucleotide on the AuNPs and the complementary sequence of the target. The different number of starting nucleation points, around which aggregation occurs, allows the discrimination between the target and the control samples.

7.2 Microfluidics experiments

7.2.1 Device optimization

The scheme of a typical microfluidic device used for all the experiments is shown in **Figure 25**. It is possible to distinguish a region where droplet generation occurs and a region where droplets are mixed. Then, the droplets reach the terminal part of the channel where fluorescence microscopy detection is performed.

As a prerequisite to using the microfluidic device, it is important to optimize device operating parameters in order to obtain a controlled droplet production. Several factors have to be taken into account in order to produce uniform droplets having a specific size and shape. The size of the channels and of the orifice where the aqueous stream merges into the non-aqueous one certainly influences the size of the

droplets. Fluids viscosity, surface tension and use of surfactants as well as hydrophobicity and hydrophilicity of the channel walls play a key role too.

The droplet generation process can be analysed in terms of the dimensionless capillary number (Ca) defined as $Ca = \mu U/\gamma$, where μ is the viscosity of the continuous phase, U is the velocity of the continuous phase, and γ is the surface tension between the water and the immiscible carrier phases. In the described case the carrier fluid (FC-3283/PFO) was injected in the main channel to act as the continuous flow while the other three inlets were filled with TRIS buffer. Flow rates of carrier fluid and immiscible aqueous solutions were adjusted in order to obtain good droplets formation. In particular, droplets having reproducible dimensions (**Figure 31**) and produced with stable frequency were obtained by both using a 10:1 mixture of FC-3283 and PFO as the carrier fluid and by maintaining carrier and aqueous solutions (inlets 1, 2 and 3) flow rates in the 1-4 μL/min and 0.1-0.3 μL/min ranges, respectively.

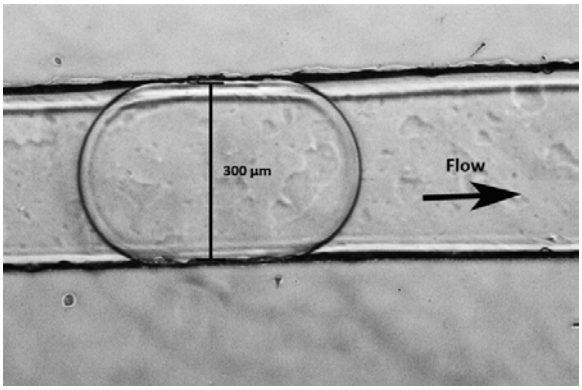

Figure 31. Optical image of a droplet.

The different amount of PFO surfactant in the carrier mixture influenced γ parameter. Increasing PFO amount in the carrier fluid lowers surface tension at the interface between droplet and carrier fluid: this raises Ca and drops form more easily.

Experimental conditions assured that droplets immediately separated from the aqueous stream at the junction where the aqueous stream met the stream of carrier fluid. Droplets generated in all microfluidic devices reported in this work were 10-20 nL in volume.

The next issue that was taken into account in device optimization was mixing of aqueous solutions inside droplets. It has been previously stated that mixing in droplets is important especially when different entities coming from different flows have to interact inside the droplet. Due to laminar flow conditions inside microfluidic channels, when two fluids come into contact with each other, there is no turbulent mixing and reagents meet only because of diffusion and although the diffusion distance is small, the time required to completely mix the two fluids could still be too long. The time (**t**) needed to mix reagents is related to both the distance **d** (μm) that a reagent must diffuse to mix with another reagent and to the diffusion coefficient **D** ($\mu m^2\ s^{-1}$) according to the equation $\mathbf{t=d^2/2D}$. In our case a mixing time in the range of minutes can be estimated. Caotic advection in winding channel has been shown to significantly accelerate mixing in droplets and for this reason a winding channel was inserted in the channel design. **Figure 32** shows the non homogeneous distribution of components encapsulated into a droplet formed when a 10^{-6} M fluorescein solution in PBS was injected into the device via inlet 3 while flowing PBS buffer through the other two inlets and carrier fluid through the main channel.

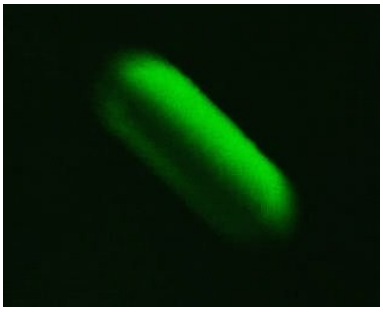

Figure 32. Image of the non homogeneous fluorescein distribution in a droplet.

7.2.2 PNA beacons

Probes used for DNA sequences identification by hybridization are peptide nucleic acids molecular beacons (MBs). They produce a fluorescent signal, due to fluorescence resonance energy transfer (FRET) mechanism, upon selectively binding to the target sequence, allowing sensitive DNA detection.

In their simpler formulation, MBs are single-stranded nucleic acid molecules that possess an hairpin structure. The loop portion of the hairpin structure is the probe sequence complementary to the target. The stem region is formed by the annealing of two complementary short sequences placed on either end of the strand. This two sequences are unrelated to the target. A fluorophore (often called reporter or donor) is attached to one end of the strand and a non-fluorescent moiety (quencher or acceptor) is attached to the other end. The stem-and-loop structure of the beacon is so that the two moieties are kept in close proximity to each other and the fluorescence of the reporter is thus quenched by fluorescence resonance energy transfer (FRET) to the quencher.

When the probe encounters the target sequence, the loop portion of the hairpin tends to hybridize with it and since the forming hybrid complex is more stable than the stem of the beacon, the hairpin unfolds and the probe stretches to hybridize completely with the target sequence. After this conformational change, the reporter is no longer in close proximity to the quencher and it emits a fluorescent signal when irradiated by the corresponding excitation wavelength (**Figure 33**).

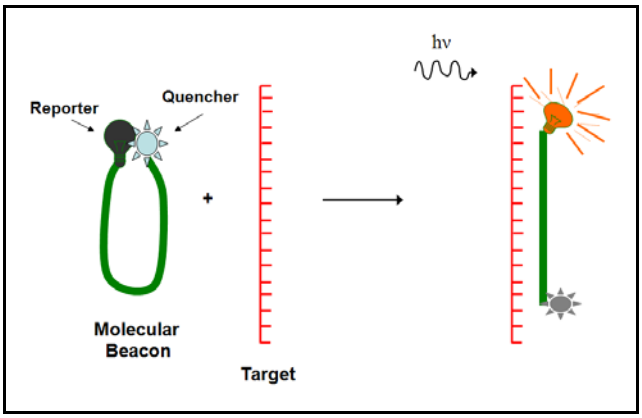

Figure 33. Molecular beacon hybridization to target sequence.

The PNA beacon used were previously synthesized according to a m odel proposed by Frank-Kamenetskii and co-workers, bearing a dabcyl unit as a quencher and fluorescein as a f luorophore, with additional oppositely charged groups and without a stem-formng sequence. It was designed to target a sequence in the actin gene of Olea europea L. which was found to contain SNP useful for variety identification. In particular, a SNP containing a T was found to be characteristic of a specific olive cultivar, namely ogliarola Leccese, while the A base was found for a wide number of other varieties.

7.2.3 Detection of synthetic oligonucleotides in a dr oplet-based microfluidics approach

The ability to detect unlabeled DNAs was preliminarily investigated by targeting a 13-mer sequence (**OGL**, **Table 1**), in the Olea europaea L. (Cultivar ogliarola) gene.

The detection was carried out by introducing both a 1 μM solution of PNA-MB in TRIS buffer (inlet 1) and the complementary **OGL** target sequence (inlet 3) into the device. Differently concentrated **OGL** solutions were injected inside the

microfluidic device one after the other, with blank registration before each sample measurement. Inlet 2 was filled with TRIS buffer. Carrier fluid (FC-3283/PFO 10:1) was injected in the main channel to act as the continuous flow. **Figure 34** shows the confidence interval of the mean at the 95% level (n=5) of the referenced fluorescence signals detected when differently concentrated **OGL** solutions were analyzed.

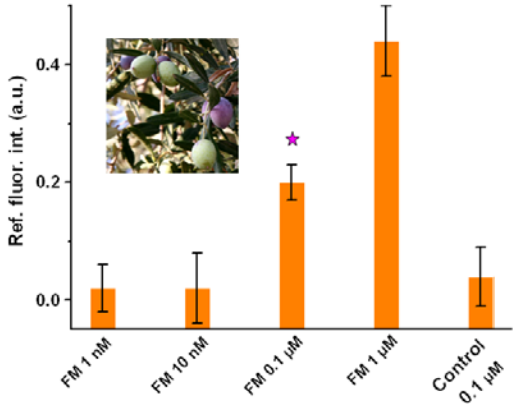

Figure 34. Referenced fluorescence intensity of synthetic oligonucleotides related to the Olea europaea L. (Cultivar ogliarola) genome (**OGL**), compared to a non-related control sequence. Error bars represent the confidence interval of the mean at the 95% level (n=5).

The ability of the system to discriminate between full-matched, single mismatched and unrelated sequences was also checked by comparing the referenced fluorescence detected when 1 µM **OGL** solutions were targeted with that detected when analyzing 1 µM sequences carrying centrally located single-base mismatch (**mOGLA, mOGLG, mOGLC**) or lateral mismatch (**mOGLT**). As can be clearly seen in **Figure 35**, no relevant signal was detected for all those sequences carrying a single centrally located single-base mismatch; these sequences behaved like the unrelated control sequence (Ctr 1 µM) and generated referenced fluorescence signals different (two-tailed t-test, level 99%, $P < 0.001$) from those generated when **OGL** full match sequence was targeted. On the other hand, the lateral location of the mutation altered the specificity of the interaction but generated referenced

fluorescence values which were still different (two-tailed t-test, level 99%, P< 0.001) than those generated by **OGL** full match sequence.

This behavior can be explained considering that when the mis-match is located near the end of a sequence, hybridization with the complementary molecular beacon is stronger than when the mis-match is in the centre. A more intense fluorescence signal is then expected.

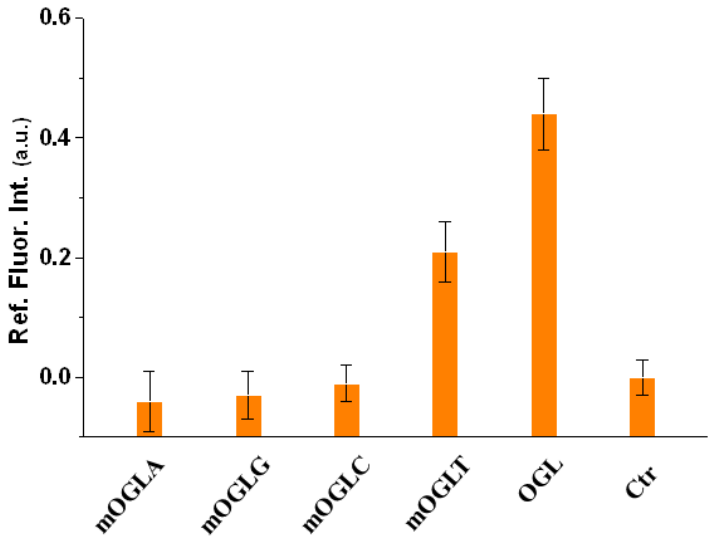

Figure 35. The referenced fluorescence intensity generated by droplets of 1 μM **OGL, mOGLA, mOGLG, mOGLC, mOGLT** and Control solutions.. Error bars represent the confidence interval of the mean at the 95% level (n=5).

These results support the enhanced PNA-MB specificity in targeting complementary sequences. In fact, even in the case of the unfavourable lateral location of the single mismatch, discrimination between full-matched sequences and mutated sequences was obtained.

7.2.4 Detection of PCR amplification products in a droplet-based microfluidic approach

Real genomic samples are usually more complex than synthetic oligonucleotide solutions. Frequently, PCR products have to be analyzed in order to detect the presence of a specific sequences in genomic DNA. Droplet-based microfluidics offers great advantages in terms of high throughput analysis and reduced sample consumption. For this reason the possibilities offered by droplet-based microfluidic devices using PNA-MBs in targeting PCR products were investigated.

The detection method so far described rely on the specific hybridization between a nucleic acid target sequence and the complementary PNA-MB. However, as far as double-stranded PCR amplicons are going to be targeted, suitable sample pre-treatments are required to obtain ssDNA available for the hybridisation with the complementary PNA-MB. DNA duplex unfolding is usually performed by keeping the sample at 95°C for 5 minutes. Once a suitable temperature for the analysis is reached, the corresponding molecular beacon can be added and signal detected. However, when the sample is to be injected in a system where it has to travel along tubes before reaching the detection point, DNA re-association can occur and thus interaction with the molecular beacon is prevented.

The adopted sample pre-treatment was based on a post-amplification strategy requiring a dsDNA high temperature denaturation step (95ºC for 5 minutes). The thermal denaturation was performed after adding OPF and OPR (**Table 1**) openers (30 μM) to the amplicon mixture. Openers were selected so as to flank the target sequence on both sides thus preventing the re-association of DNA strands before the interaction between the PNA-MB probe and the target sequence (**Figure 36**).

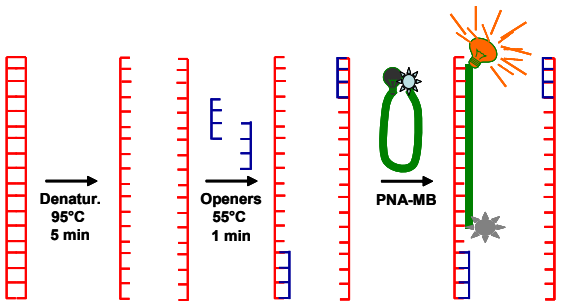

Figure 36. Schematic representation of the procedure adopted to allow the target sequence to be locally exposed to the PNA-MB complementary probe.

OPF and OPR hybridization with the complementary sequences was favoured by maintaining the mixture containing the denatured PCR product at a temperature close to the openers annealing temperature (55ºC, 1 min.). The pre-treated sample solutions were then injected into the microfluidic device for droplets formation and PNA-MB targeting.

Figure 37 shows the confidence intervals of the mean at the 95% level (n=5) of the referenced fluorescence signals detected when droplets of pre-treated 10 nM PCR amplicon of DNAs extracted from leaves of two different cultivars (C. Ogliarola and C. Ascolana) of *Olea europaea L.* were analyzed by using **PNA-MB**. The C. Ogliarola targeted sequence differs by a T→A SNP from other varieties. The **PNA-MB** targeting allowed the 10 nM C Ogliarola amplicon solution to be discriminated (two-tailed t-test, level 99%, ν=8, $P < 0.01$) from both the 10 nM C. Ascolana amplicon as well as the blank solutions.

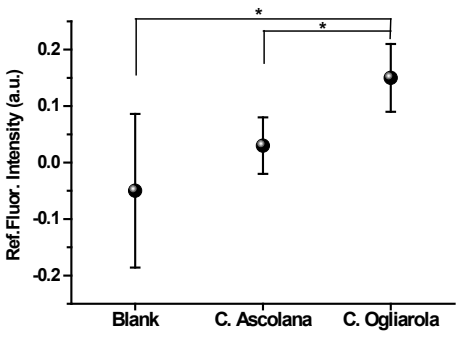

Figure 37. Confidence intervals of the mean (95% level, n=5) of the referenced fluorescence signals detected when droplets of pre-treated 10 nM PCR amplicon of DNAs extracted from leaves of Olea europaea L. Ogliarola and Ascolana cultivars were detected (* two-tailed t-test, level 99%, v=8, P< 0.01).

The 10 nM sensitivity of **PNA MB** can be combined with the possibilities offered by the droplet-based analytical approach. In fact, dozens of droplets can be generated by using less than 1 µl of sample and since analyzed droplets were between 10-20 nL in volume, it can be estimated that 100-200 attomoles of dsDNA PCR amplicons were involved in the detection process.

7.2.5 Circular strand displacement polymerization reaction

The principle of the isothermal amplified detection DNA method is shown in **Figure 21**. This DNA detection system consists of a hairpin fluorescence probe with a stem-loop structure, a short primer and polymerase. A fluorophore (6-FAM) and a quencher (BHQ-1) are linked to the ends of the stem of the hairpin fluorescence probe. In the absence of a target, the probe is unable to anneal with the primer to induce a polymerization reaction. However, in the presence of the complementary target sequence, the probe hybridizes with it and undergoes a conformational change, leading to stem separation. Then, the primer anneals with the open stem and triggers a polymerization reaction in the presence of dNTPs/polymerase. A complementary

DNA is synthesized, forming a probe–cDNA complex while the target is displaced by the polymerase with strand-displacement activity. All the steps are carried out in a cyclical process where the hairpin fluorescence probe plays a key role as both template of polymerization reaction and fluorescence signal carrier, while the target acts as a trigger of polymerization reaction.

The activation of the DNA system is based on the conformational change of the hairpin fluorescence probe upon hybridization with target DNA. The system is able to detect the target with high sensitivity because even minute amounts of targets can produce fluorescence enhancement.

In order to evaluate the capability of the hairpin fluorescence probe to selectively recognize and hybridize with the complementary target sequence, reaction mixtures containing the full-match target oligonucleotide related to to the genetically modified Roundup Ready soybean genome and the random single-stranded DNA (control DNA) oligonucleotide were incubated at 37 °C out of the device for 20 minutes or 1 hour and then injected in the microchannel. **Figure 38** shows the referenced fluorescence intensities observed when experiments were performed with 0.12 μM probe and 11 nM target or control DNAs. The results implied that the hairpin fluorescence probe underwent a conformational change only upon hybridization with the target and that fluorescence was restored. Therefore, the hairpin fluorescence probe was suitable to act as a template for polymerization reaction in this study. Conversely, the control experiment performed with addition of random single-stranded DNA revealed that polymerization reaction was not triggered even in the presence of dNTPs/polymerase, implying that the detection was target-specific.

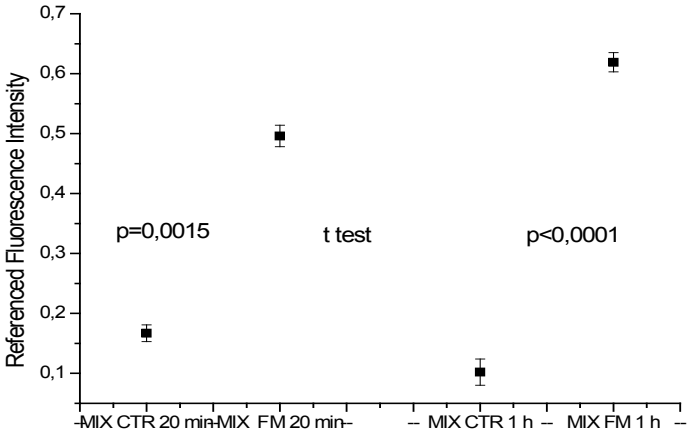

Figure 38. Referenced Fluorescence Intensity of synthetic oligonucleotides related to Roundup Ready soybean genome, compared with random (negative control) sequences.

Having proved the suitability of the described approach for the detection of DNA amplification when the polymerization reaction was performed out of the microchannel and at a optimal temperature (37°C), the feasibility of the method was then investigated when the amplification was allowed to occur inside the microchannel. **Figure 39** shows the change of fluorescence intensities over time for the target oligonucleotide related to Roundup Ready soybean genome and the random (negative control) sequence. The fluorescence intensity for the target maintained its increase with time, indicating the conformational change of the hairpin fluorescence probe and the continuous formation of probe–cDNA complex as a result of circular polymerization reaction. In the presence of the control sequence, a little fluorescence intensity change was observed, indicating that no polymerization reaction was triggered.

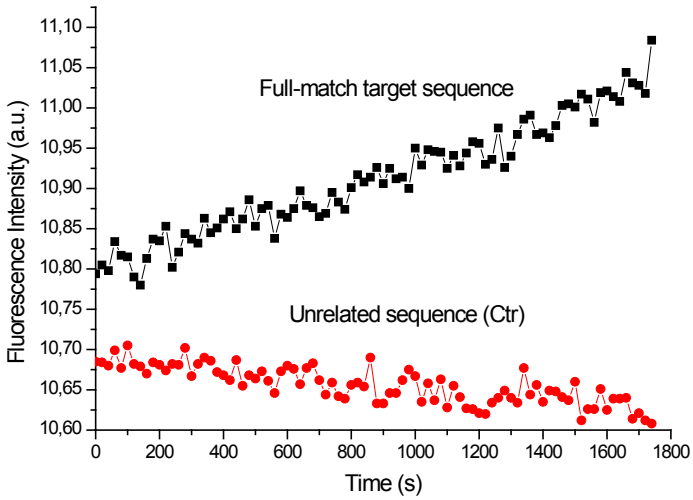

Figure 39. Verification of isothermal strand-displacement polymerization reaction in a mixture with 11 nM target and Ctr DNA.

8. CONCLUSIONS

During my PhD I investigated new tools to be used for DNA detection with the principal aim to perform the analysis with a limited number of sample molecules. In particular, two fields were investigated: i) the ultrasensitive DNA detection obtained by using the metallic nanoparticle-enhanced surface plasmon resonance sensing and ii) droplet-based microfluidics.

SPRi results show that the used approach allows the discrimination between normal and mutated sequences even in the case of single-nucleotide mutation. This study represents the first demonstration of SPRi ultrasensitive detection of point mutation using non-amplified genomic DNA isolated from patients affected by an hereditary genetic disease. It has been shown that homozygous and heterozygous DNA samples carrying the β°39 point mutation are discriminated both from each other and from normal DNA samples. It is important to underline that the discrimination was obtained at a very low concentration (2.6 aM). With this concentration, not only it is possible to avoid the PCR amplification of nucleic acids, but it would be also possible to perform genetic studies for prenatal diagnosis directly on fetal DNA extracted from maternal blood, thus contributing to the replacement of most of the other currently used approaches requiring invasive procedures such as amniocentesis, chorionic villous sampling or fetal blood sampling, each associated to a small but finite risk of fetal loss.

In addition, the described approach is convenient, requiring only sonication and denaturation of genomic DNA samples, minimizing the possibility to contaminate the DNA samples to be analyzed.

A droplet-based microfluidic approach based on a combination of PNA molecular beacons and fluorescence microscopy has been described for the analysis of ssDNA and PCR amplicons. The ability of these systems in detecting DNA molecule in different samples was investigated starting with ideal oligonucleotide sequences in the Olea europaea L. (Cultivar ogliarola) genome and proceeding then with real PCR amplification samples, with the injection of just 1 μl of sample. It has been shown that it is possible to detect synthetic oligonucleotides down to 100 nM concentration with the digital microfluidic devices used in this work. Detection is specific since unrelated or even single mis-matched sequences produce no relevant signal. Mis-matched sequences can be distinguished in terms of mis-match position along the sequence since a higher fluorescence enhancement is observed when the mis-match is close to the end of the sequence.

The analysis of symmetric PCR amplification products confined in aqueous droplets required a specific sample pre-treatment to be set up in order to obtain ssDNA sequences from the dsDNA PCR amplification products available for PNA-MB targeting. The procedure allowed the fluorescence detection from droplets of 10 nM PCR amplification products of DNA samples extracted from leaves of Olea europaea L.(Cultivar ogliarola). The fluorescence data were compared with those obtained analysing the PCR amplicon from a different Olea europaea L. cultivar (Ascolana) carrying a single base polymorphism (SNP) in the target sequence.

Non-specific interactions with substrate surface and slow diffusion issues, commonly encountered with biosensors, are avoided with this microfluidic application because interaction between probe and target sequence occurs in solution, and droplets can be easily manipulated and thoroughly mixed inside the microfluidic channels.

A method with a novel platform based on polymerase-induced isothermal strand-displacement polymerization reaction was also presented which simultaneously amplifies and detects ssDNA. The approach allowed to detect 11 nM oligonucleotide sequences by using about 100 fmol of sample.

RESULTS OF THE RESEARCH ACTIVITY: PUBLICATIONS

Zanoli, L.; D'Agata, R.; Spoto, G. *Minerva Biotecnol.* **2008**, *20(4)*, 165-174.

Grasso, G.; D'Agata, R.; Zanoli, L.; Spoto, G. *Microchem. J.* **2009**, *93*, 82–86.

D'Agata, R.; Corradini, R.; Ferretti, C.; Zanoli, L.; Gatti, M.; Marchelli, R.; Spoto, G. *Biosens. Bioelectron*. **2010**, *25*, 2095–2100.

D'Agata, R.; Corradini, R.; Ferretti, C.; Zanoli, L.M.; Gatti, M.; Marchelli, R.; Spoto, G. *Chim. Ind. (Milan)* **2010**, *92(7)*, 140-145

Zanoli, L.M.; D'Agata, R.; Corradini, R.; Ferretti, C.; Gatti, M.; Marchelli, R.; Spoto, G. In *Lecture Notes in Electrical Engineering*, Neri, G.; Donato, N.; D'Amico, A.; Di Natale, C., Ed.; Springer, 2011; Vol. 91, pp 485-488.

D'Agata, R.; Breveglieri, G.; Zanoli, L.M.; Borgatti, M.; Spoto S.; Gambari, R. *Anal. Chem.* **2011**, *83 (22),* 8711–8717.

Zanoli, L.M.; D'Agata, R. Spoto, G. *Anal. Bioanal. Chem. Springer-Verlag* **2011**, DOI 10.1007/s00216-011-5318-3.A. (Selected Hot Article)

Zanoli, L.M.; Licciardello, M.; D'Agata, R.; Lantano, C.; Calabretta, A.; Corradini, R.; Marchelli, R.; Spoto, G. *Anal. Bioanal. Chem. Springer-Verlag,* **2011**, in press.

ACKNOWLEDGEMENTS

I would like to express my deep and sincere gratitude to Prof. Giuseppe Spoto, for his encouraging and personal guidance, and also to Dr. Giuseppe Grasso, Dr. Roberta D'Agata and Dr. Marco Licciardello, for their friendship and continuous support.

They are like family to me.

REFERENCES

[1] Shi, L.; Perkins, R.G.; Fang, H.; Tong, W. *Curr. Opin. Biotechnol.* **2008**, *19*, 10–18.

[2] Cooper, M.A. *Nat. Rev. Drug discov.* **2002,** *1,* 515-528.

[3] Homola, J.; Yee, S.S.; Gauglitz, G. *Sensor Actuator B Chem.* **1999,** *B54(1-2),* 3-15.

[4] Homola, J. *Anal. Bioanal. Chem.* **2003,** *377,* 528-539.

[5] Goodrich, T.T.; Lee, H.J.; Corn, R.M. *J. Am. Chem. Soc.* **2004,** *126,* 4086-4087.

[6] Song, F.; Zhou, F.; Wang, J.; Nongjian, T.; Jianiao, L.; Vellanoweth, R.L.; Morquecho, Y.; Wheeler-Laidman, J. *Nucleic Acids Res.* **2002,** *30,* e72.

[7] Fang, S.; Lee, H.J.; Wark, A.W.; Corn, R.M. *J. Am. Chem. Soc.* **2006,** *128,* 14044-14046.

[8] Ito, M.; Nakamura, F.; Baba, A.; Tamada, K.; Ushijima, H.; Lau, K.H.A.; Manna, A.; Knoll, W. *J. Phys. Chem. C* **2007,** *111,* 11653-11662.

[9] D'Agata, R.; Corradini, R.; Grasso, G.; Marchelli, R.; Spoto, G. *ChemBioChem* **2008,** *9,* 2067-2070.

[10] Rossi, S.; Scaravelli, E.; Germini, A.; Corradini, R.; Fogher, C.; Marchelli, R. A *Eur. Food Res. Techol.* **2006,** *23,* 1-6.

[11] Homola J. *Chem. Rev*. **2008**, *108*, 462-493.

[12] Wood, R.W. *Philos. Mag.* **1902**, *4*, 396–402.

[13] Wood, R.W. *Philos. Mag*. **1912**, *23*, 310–317.

[14] Rayleigh, L. *Proc. R. Soc. Lon.* A, **1907**, *79*, 399-416.

[15] Fano, U. *J. Opt. Soc. Am.* **1941**, *31*, 213–222.

[16] Otto, A. *Zeits Phys.* **1968**, *216*, 398–410.

[17] Kretschmann, E.; Reather, H. *Z. Naturforsch.* **1968**, *23*, 2135–2136.

[18] Pockrand, I.; Swalen, J.D.; Gordon, J.G.; Philpott, M.R. *Surf. Sci.* **1978**, *74*: 237-244.

[19] Gordon, J.G.; Ernst, S. *Surf. Sci.* **1980**, *101*, 499-506

[20] Liedberg, B.; Nylander, C.; Lundstrom, I. *Sens. Actuators* **1983**, *4*, 299–304.

[21] Jonsson, U.; Fagerstam, L.; Ivarsson, B.; Johnsson, B.; Karlsson, R.; Lundh, K.; Lofas, S.; Malmqvist, M. *BioTechniques* **1991**, *11*, 620–627.

[22] Kooyman, R.P.H. In: *Handbook of surface plasmon resonance*, Schasfoort, R.B.M. and Tudos, A.J., Ed.; The Royal Society of Chemistry: Cambridge, 2008; pp. 15-34.

[23]Raether, H., Surface Plasmons on smooth and rough surfaces and on gratings, Springer-Verlag, Berlin, **1988.**

[24]Powell, C. J.; Swan, J. B. *Phys. Rev.* **1960**, *118,* 640-643.

[25]Agranovich, V. M.; Mills, D. L. Surface Polaritons, North HollandCo., Amsterdam, **1982**.

[26] Kretschmann, E. *Z. Phys.* **1971**, *241*, 313–324.

[27]Matsubara, K.; Rawata, S.; Minami S. *Opt. Let.* **1990**, *15*, 75-77.

[28]Forstamann, F.; Gerhardts, R.R. Metal Optics Near the Plasma Frequency, Springer, Tracts in Modern Physics, **1986**, Vol.*109*.

[29]Akimoto, T.; Sasaki, S.; Ikebukuro, K.; Karube, I. *Biosens. Bioelectron*. **2000**, *15*, 355-362.

[30] a) Rich, R.L.; Myszka, D.G. *Curr. Opin. Biotechnol.* **2000**, *11,* 54-61; (b) Quinn, J.G.; O'Neill, S.; Doyle, A.; McAtamney, C.; Diamond, D.; MacCraith, B.D.; O'Kennedy, R. *Anal. Biochem.* **2000**, *281*, 135-143; (c) Myszka, D.G.; Rich, R.L., *Pharm. Sci. Technol*. *Today* **2000**, *3*, 310-317.

[31] Frutos, A.G.; Weibel, S.C.; Corn R.M. *Anal. Chem.* **1999**, *71*, 3935-3940.

[32] (a) Baird, C.L.; Courtenay, E.S.; Myszka, D.G. *Anal. Biochem.* **2002**, *310*, 93-99; (b) Evans, S.V.; MacKenzie C.R. *J. Mol. Recognit.* **1999**, *12*, 155-168; (c) Karlsson, R. *Anal. Biochem.* **1994**, *221*, 142-151; (d). Nilsson, P.; Persson, B.; Uhlen, M.; Nygren, P.A. *Anal. Biochem.* **1995**, *224*, 400-408.

[33] Tumolo T.; Angnes L.; Baptista M.S. *Anal. Biochem.* **2004,** *333*, 273–279.

[34] Oshannessy, D.J. ; Brighamburke, M. ; Soneson, K.K. ; Hensley, P. ; Brooks, I. *Anal. Biochem.* **1993,** *212*, 457-468.

[35] Jonsson, U. Fägerstam, L. ; Ivarsson, B. ; Johnsson, B. ; Karlsson, R. ; Lundh, K. ; Löfås, S. ; Persson. B. *Biotechnique* **1991**, *11*, 620-627.

[36] O'Shannessy, D.J.; Winzor, D.J. *Anal. Biochem.* **1996**, *236*, 275-283.

[37] Karlsson R.; Michaelsson A.; Mattson L. *J. Immunol. Methods*, **1991**, *145*, 229-240.

[38] Fisher, R.J.; Fivash, M.; Casas-Finet, J.; Erickson, J.W.; Kondoh, A.; Bladen, S.V.; Fisher, C.; Watson, D.K.; Papas, T. *Protein Sci.* **1994**, *3*, 257-266.

[39] Karlsson, R.; Falt, A. *J. Immunol. Methods* **1997,** *200*, 21-133.

[40] Goodrich, T.T.; Wark, A.W.; Corn, R.M.; Lee, H.J. In *New and E merging Proteomic Techniques,* Nedelkov, D. and Nelson, R.W., Ed.; Humana Press Inc.: Totowa, NJ, 2006; Vol. 328, pp 113-130.

[41] Wark, A.W.; Lee, H.J.; Corn, R.M. *Angew. Chem. Int. Ed.* **2008,** *47*, 644-652

[42] Lee, H.J.; Wark, A.W.; Corn, R.M. *Langmuir* **2006**, *22*, 5241-5250

[43] Smith, E.A.; Corn, R.M**.** *Appl. Spectrosc.* **2003,** *57,* 320A-332A.

[44] Steiner, G. *Anal. Bioanal. Chem.* **2004,** *379,* 328-331.

[45] Malmqvist, M. *Nature* **1993**, *361*, 186-187.

[46] Rothenhäusler, B.; Knoll, W. *Nature* **1988**, *332*, 615-617.

[47] (a) Brockman, J.M.; Nelson, B.P.; Corn, R.M. *Annu. Rev. Phys. Chem*. **2000**, *51*, 41–63; (b) Smith, E.A.; Corn, R.M.; *Appl. Spect*. **2003**, *57*, 320–332.

[48] Kanoh, N.; Kyo, M.; Inamori, K.; Ando, A.; Asami, A.; Nakao, A.; Osada, H. *Anal. Chem.* **2006**, *78(7),* 2226-2230.

[49] Shumaker-Parry, J.S.; Campbell, C.T. *Anal. Chem.* **2004**, *76,* 907-917.

[50] Shumaker-Parry, J.S.; Aebersold, R.; Campbell, C.T. *Anal. Chem.* **2004**, *76,* 2071-2082.

[51] Scarano, S.; Mascini, M.; Turner, A.P.F.; Minunni, M. *Biosens. Bioelectron*. **2010**, *25(5),* 957-966.

[52] He, L.; Musick, M.D.; Nicewarner, S.R.; Salinas, F.G.; Benkovic, S.J.; Natan, M.J.; Keating, C.D. *J. Am. Chem. Soc.* **2000**, *122*, 9071-9077.

[53] Kubitschko, S.; Spinke, J.; Bruckner, T.; Pohl, S.; Oranth, N. *Anal. Biochem*. **1997**, *253*, 112-122.

[54] Taton, T. A.; Mirkin, C.A.; Letsinger, R.L. *Science* **2000**, *289*, 1757-1760.

[55] Yao, X.; Li, X.; Toledo, F.; Zurita-Lopez, C.; Gutova, M.; Momand, J.; Zhou, F.; *Anal. Biochem*. **2006**, *354*, 220–228.

[56] Russom, A.; Haasl, S.; Brookes, A.J.; Andersson, H.; Stemme, G.; *Anal. Chem.* **2006**, *78*, 2220-2225.

[57] Hu, Y.J.; Li, Z.F.; Diamond, A.M. *Anal. Biochem*. **2007**, *369*, 54–59.

[58] Li, Y.; Wark, A.W.; Lee, H.J.; Corn, R.M. *Anal. Chem.* **2006**, *78*, 3158-3164.

[59] Zanoli, L.; D'Agata, R.; Spoto, G. *Minerva Biotecnol.* **2008**, *20,* 165-174.

[60] Nielsen, P.E.; Egholm, M.; Berg, R.H.; Buchardt, O. *Science* **1991**, *254*, 1497-1500.

[61] Nielsen, P. *Q. Rev. Biophys* **2005**, *38*, 345-350.

[62] (a) Gao, Z.; Agarwal, A.; Trigg, A.D.; Singh, N.F.; Cheng, T.; Yi, C.H.F.; Buddharaju, D.K.; Kong, J. *Anal. Chem.* **2007**, *79*, 3291-3297; (b) Li-Qiang, C.; Foerch, R.; Knoll, W. *Angew. Chem. Int. Ed*. **2007**, *46*, 4944-4947; (c) Liu, J.; Tiefenauer, L.; Tian, S.; Nielsen, P.E.; Knoll, W. *Anal. Chem.* **2006**, *78*, 470-476.

[63] Gambari R. *Curr. Pharm. Des.* **2001**, *7*, 1839-62.

[64] Jensen, K.K.; Ørum, H.; Nielsen, P.E.; Norden, B. *Biochemistry* **1997**, *36*, 5072-5077.

[65] Nielsen, P.E.; Egholm, M. Bioorg. *Med. Chem.* **2001**, *9*, 2429–2434.

[66] Kurakin, A.; Larsen, H.J.; Nielsen, P.E. *Chem. Biol.* **1998**, *5,* 81-89.

[67] Sawata, S.; Kai, E.; Ikebukuro, K.; Iida, T.; Honda, T.; Karube, I. *Biosens. Bioelectron*. **1999**, *14*, 397-404.

[68] Kai, E.; Ikebukuro, K.; Hoshina, S.; Watanabe, H.; Karube, I. *FEMS Immunol. Med. Microbiol.* **2000**, *29*, 283-288.

[69] Chilkoti, A.; Stayton, P.S. *J. Am. Chem. Soc.* **1995**, *117*, 10622-10628.

[70] Burgener, M.; Sänger, M.; Candrian, U. *Bioconjugate Chem.* **2000**, *11*, 749-754.

[71] Whitesides, G.M. *Nature* **2006,** *422,* 368-373.

[72] Stone, H.A.; Stroock, A.D.; Ajdari, A. *Annu. Rev. Fluid Mech.* **2004**, *36*, 381–411.

[73] Griffiths, A.D.; Tawfik, D.S. *Trends Biotechnol*. **2006**, *24*, 395–402.

[74] Fair, R.B. *Microfluidics Nanofluidics*, **2007**, *3*, 245–281.

[75] Teh, S-Y.; Lin, R.; Hung, L.H.; Lee, A.P. *Lab Chip,* **2008**, *8*, 198–220.

[76] Christopher, G.F.; Anna, S.L. *J. Phys. D: Appl. Phys.* **2007,** *40,* R319–R336.

[77] Song, H.; Chen, D.L.; Ismagilov, R.F. *Angew. Chem. Int. Ed*. **2006**, *45*, 7336–56

[78] Jensen, K.; Lee, A. *Lab Chip* **2004,** *4*, 31N–2N.

[79] Xu, S. Q.; Nie, Z.H.; Seo, M.; Lewis, P.; Kumacheva, E.; Stone, H.A.; Garstecki, P.; Weibel, D.B.; Gitlin, I.; Whitesides, G.M. *Angew. Chem*. **2005**, *117*, 734–738.

[80] Martin, K.; Henkel, T.; Baier, V.; Grodrian, A.; Schon, T.; Roth, M.; Kohler, J. M.; Metze, J. *Lab Chip* **2003**, *3*, 202–207.

[81] Cho, W.; Ko, Y.-J.; Ahn, Y.; Yoon, J.-Y.; Cho, N.G. *Key Eng. Mater.* **2006**, 326–328, 297–300.

[82] Hu, S.W.; Ren, X.Q.; Bachman, M.; Sims, C.E.; Li, G.P.; Allbritton, N.L. *Anal. Chem.* **2004**, *76*, 1865–1870.

[83] Xu, J.H.; Li, S.W.; Tan, J.; Wang, Y.J.; Luo, G.S. *AIChE J.* **2006**, *52*, 3005–3010.

[84] Thorsen, T.; Roberts, R.W.; Arnold, F.H.; Quake, S.R. *Phys. Rev. Lett*. **2001**, *86*, 4163–4166.

[85] Yobas, L.; Martens, S.; Ong, W.L.; Ranganathan. N. *Lab Chip* **2006**, *6*, 1073–1079.

[86] Anna, S.L.; Bontoux, N.; Stone, H.A. *Appl. Phys. Lett,* **2003**, *82,* 364–366.

[87] Ahmed, R.; Jones, T.B. *J. Electrost.* **2006***, 64,* 543–549.

[88] Wang, K.L.; Jones, T.B.; Raisanen, A. *J. Micromech. Microeng.* **2007**, *17,* 76–80.

[89] Jang, L.S.; Lin, G.H.; Lin, Y.L.; Hsu, C.Y.; Kan, W.H.; Chen, C.H. *Biomed. Microdev.* **2007***, 9,* 777–786.

[90] He, M.; Kuo, J.S.; Chiu, D.T. *Langmuir,* **2006***, 22,* 6408–6413.

[91] Brody, J.; Yager, P.; Goldstein, R.; Austin, R. *Biophys. J.* **1996**, *71,* 3430–3441

[92] Beebe, D.J.; Mensing, G.A.; Walker, G.M. *Annu. Rev. Biomed. Eng.* **2002***, 4,* 261–286

[93] Janasek, D.; Franzke, J.; Manz. A. *Nature* **2006**, *442*, 374-380.

[94] Reynolds, O. *Phil. Trans. R. Soc. Lond.* **1883**, *174*, 935–982.

[95] Squires, T.M.; Quake, S.R. *Rev. Mod. Phys.* **2005**, *77,* 977–1026.

[96] Stone, H.A. *Ann. Rev. Fluid Mech*. **1994**, *26*, 65-102.

[97] Tice, J.D.; Song, H.; Lyon, A.D.; Ismagilov, R.F. *Langmuir* **2003**, *19*, 9127-9133

[98] Nisisako, T.; Okushima, S.; Torii, T. *Soft Matter*, **2005**, *1*, 23–27.

[99] Anna, S.L.; Mayer, H.C. *Phys. Fluids* **2006**, *18*, 121512.

[100] Pihl, J.; Karlsson, M.; Chiu, D.T. *DDT* **2005**, *10 (20)*, 1377-1383.

[101] Stroock, A.D.; Dertinger, S.K.W.; Ajdari, A.; Mezić, I.; Stone, H.A.; Whitesides, G.M. *Science* **2002,** *295*, 647–651.

[102] Song, H.; Ismagilov, R.F. *J. Am. Chem. Soc.* **2003**, *125*, 14613–14619.

[103] DeMello, A.J. *Nature* **2006**, *442*, 394-402

[104] Handique, K.; Burns, M.A. *J. Micromech. Microeng.* **2001**, *11*, 548–554.

[105] Bringer, M.R.; Gerdts, C.J.; Song, H.; Tice, J.D.; Ismagilov, R.F. *Phil. Trans. R. Soc. Lond. A* **2004**, *362*, 1087–1104.

[106] Paik, P.; Pamula, V.K.; Pollack, M.G.; Fair, R.B. *Lab Chip* **2003**, *3*, 28–33.

[107] Song, H.; Tice, J.D.; Ismagilov, R.F. *Angew. Chem. Int. Ed.* **2003**, *42*, 768 – 772.

[108] Fidalgo, L.M.; Abell, C.; Huck, W.T.S. *Lab Chip* **2007**, *7*, 984–986.

[109] Tan, Y.-C.; Ho, Y.; Lee, A. *Microfluidics Nanofluidics* **2007**, *3*, 495–499.

[110] Liu, K.; Ding, H.J.; Chen, Y.; Zhao, X.Z. *Microfluidics Nanofluidics* **2007**, *3*, 239–243.

[111] Tan, Y.C; Ho, Y.L; Lee, A.P. Microfluid Nanofluid 2008, 4, 343–348

[112] Tan, Y.C.; Fisher, J.S.; Lee, A.I.; Cristini, V.; Lee, A.P. *Lab Chip* **2004**, *4*, 292–298.

[113] Agresti, J.J.; Antipov, E.; Abate, A.R.; Ahn, K.; Rowat, A.C.; Baret, J.C.; Marquez, M.; Klibanov, A.M.; Griffiths, A.D.; Weitz, D.A. *PNAS* **2010**, *107 (9)*, 4004–4009

[114] Faraday, M. *Philos. Trans. R. Soc. London* **1857,** *147*, 145–181.

[115] Mie, G. *Ann. Phys.* **1908**, *25*, 377–445

[116] Ghosh, S.K.; Pal, T. *Chem. Rev.* **2007**, *107*, 4797–4862

[117] Rosi, N.L.; Mirkin, C.A. *Chem. Rev.* **2005**, *105*, 1547–1562

[118] Mrinmoy, D.; Ghosh, P.S.; Rotello, V.M. *Adv. Mater.* **2008**, *20*, 4225–4241.

[119] Niemeyer, C.M. *Angew. Chem. Int. Ed.* **2001**, *40*, 4128–4185.

[120] Seeman, N.C. *Trends Biotechnol*. **1999**, *17*, 437–443.

[121] Niemeyer, C.M. *Curr. Opin. Chem. Biol.* **2000**, *4*, 609–618.

[122] Zhao, W.; Brook, M.A.; Li, Y.F. *ChemBioChem* **2008**, *9*, 2363–2371

[123] Daniel, M.C.; Astruc, D. *Chem. Rev.* **2004**, *104*, 293–346.

[124] Green, M. *Chem. Commun*. **2005**, *24*, 3002–3011.

[125] Murphy, C.J.; San, T.K.; Gole, A.M.; Orendorff, C.J.; Gao, J.X.; Gou, L.; Hunyadi, S.E.; Li, T. *J. Phys. Chem. B* **2005**, *109*, 13857–13870.

[126] Turkevich, J.; Stevenson, P.C.; Hillier, J. *Discuss. Faraday Soc.* **1951**, *11*, 55–75.

[127] Baptista, P.; Pereira, E.; Eaton, P.; Doria, G.; Miranda, A.; Gomes, I.; Quaresma, P.; Franco, R. *Anal. Bioanal. Chem.* **2008**, *391*, 943–950.

[128] Frens, G. *Nature* **1973**, *241*, 20–22.

[129] Wilson, R. *Chem. Soc. Rev.* **2008**, *37*, 2028–2045.

[130] Li, H.; Rothberg, L. *PNAS* **2004**, *101*, 14036–14039

[131] Yang-Wei, L.; Chi-Wei, L.; Huan-Tsung, C.; *Anal. Methods* **2009**, *1*, 14–24.

[132] Cioffi, N.; Colaianni, L.; Ieva, E.; Pilolli, R.; Ditaranto, N.;, Angione, M.D.; Cotrone, S.; Buchholt, K.; Spetz, A.L.; Sabbatini, L.; Torsi, L. *Electrochim. Acta* **2011**, *56*, 3713–3720.

[133] Ojea-Jiménez, I.; Puntes, V. *J. Am. Chem. Soc.*, **2009**, *131* (37), 13320–13327.

[134]Hermanson, G.H. In *Bioconjugated techniques*, Elsevier Academic Press: Amsterdam, 2008; pp 924-935

[135] Van Driessche, I.; Hoste, S. In *Functional coatings: by polymer microencapsulation*, Ghosh, S.K., Ed.; Wiley & Sons Ltd.: Weinheim, 2006; pp 259-296.

[136] Bastús, N.G.; Casals, E.; Vázquez-Campos, S.; Puntes, V. *Nanotoxicology* **2008**, *2*, 99–112.

[137] Weisbecker, C.S.; Merritt, M.V.; Whitesides, G.M. *Langmuir* **1996**, *12*, 3763–3772.

[138] Norde, W. *Adv. Colloid Interface Sci.* **1986**, *25*, 267-340.

[139] Norde, W.; MacRitchie, F.; Nowicka, G.; Lyklema, J. *J. Colloid Interface Sci.* **1986**, *112 (2)*, 447-456

[140] Mirkin, C.A.; Letsinger, R.L.; Mucic, R.C.; Storhoff, J.J. *Nature* **1996**, *382*, 607–609.

[141] Pellegrino, T.; Kudera, S.; Liedl, T.; Javier, A.M.; Manna, L.; Parak, W.J. *Small* **2005**, *1*, 48–63

[142] Peña, S.R.N.; Raina, S.; Goodrich, G.P.; Fedoroff, N.V.; Keating, C.D. *J. Am. Chem. Soc.* **2002**, *124*, 7314–7323.

[143] Hurst, S.J.; Lytton-Jean, A.K.R.; Mirkin, C.A. *Anal. Chem*. **2006**, *78*, 8313–8318.

[144] Jin, R.; Wu, G.; Li, Z.; Mirkin, C.A.; Schatz, G.C. *J. Am. Chem. Soc.* **2003**, *125*, 1643-1654.

[145] Sperling, R.A.; Gil, P.R.; Zhang, F.; Zanella, M.; Parak, W.J. *Chem. Soc. Rev.* **2008**, *37*, 1896–1908.

[146] Alivisatos, A.P.; Johnsson, K.P.; Peng, X.; Wilson, T.E.; Loweth, C.J.; Bruchez, M.P.; Schultz, P.G. *Nature* **1996**, *382*, 609–611.

[147] D'Agata, R.; Corradini, R.; Ferretti, C.; Zanoli, L.; Gatti, M.; Marchelli, R.; Spoto, G. *Biosens. Bioelectron.* **2010**, *25*, 2095–2100.

[148] Merkoçi, A. *Biosens. Bioelectron.* **2010**, *26*, 1164–1177.

[149] Pérez-López, B.; Merkoçi, A. *Anal. Bioanal. Chem.* **2011**, *399*, 1577–1590.

[150] Xia, Y.; Whitesides, G. *Angew. Chem.* **1998**, *37*, 550-575.

[151] Jung, L.S.; Campbell, C.T.; Chinowsky, T.M.; Mar, M.N.; Yee, S.S. *Langmuir* **1998**, *14*, 5636-5648.

[152] Grabar, K.C.; Freeman, R.G.; Hommer, M.B.; Natan, M.J. *Anal. Chem.* **1995**, *67*, 735–743.

[153] Haiss, W.; Thanh, N.T.K.; Aveyard, J.; Fernig, D.G. *Anal. Chem.* **2007**, *79*, 4215–4221.

[154] Totsingan, F.; Rossi, S.; Corradini, R.; Tedeschi, T; Sforza, S.; Juris, A.; Scaravelli, E.; Marchelli, R. *Org. Biomol. Chem.* **2008**, *6*, 1232-1237.

[155] Doyle, J.J. Doyle, J.L. *Phytochem. Bull.* **1987**, 19, 11-15

[156] Wang, R.; Minunni, M.; Tombelli, S.; Mascini, M. *Biosens. Biolectron***. 2004***, 20*, 598-605

[157] Guo, Q.; Yang, X.; Wang, K.; Tan, W.; Li, W.; Tang, H.; Li, H. *Nucleic Acids Res.,* **2009***, 37*, No. 3 e20

[158] Grasso, G.; D'Agata, R.; Zanoli, L.; Spoto, G. *Microchem. J.* **2009**, *93*, 82-86

[159] Tice, J.D.; Lyon, A.D.; Ismagilov, R.F. *Anal. Chim. Acta* **2004**, *507*, 73-77.

[160] Roach, L.S.; Song, H.; Ismagilov, R.F. *Anal. Chem.* **2005**, *77*, 785-796.

[161] Myszka, D.G. *J. Mol. Recognit.* **1999,** 12**,** 279–284

[162] Park, H.; Germini, A.; Sforza, S.; Corradini, R.; Marchelli, R.; Knoll, W. *Biointerphases* **2007***, 2*, 80-88.

[163] Peterson, A.W.; Wolf, L.K.; Georgiadis, R.M. *J. Am. Chem. Soc.* **2002**, *124*, 14601-14607.

[164] Peterson, A.W.; Heaton, R.J.; Georgiadis, R.M. *Nucleic Acids Res.* **2001***, 29,* 5163-5168.

[165] International Human Genome Sequencing Consortium, *Nature* **2001**, *409*, 860-921.

[166] Venter, J.C. et al., *Science* **2001,** *291*, 1304-1351.